

## Review

Wu Zhang, Haizeng Li\*, Eric Hopmann and Abdulkhakem Y. Elezzabi\*

# Nanostructured inorganic electrochromic materials for light applications

<https://doi.org/10.1515/nanoph-2020-0474>

Received August 13, 2020; accepted November 6, 2020;

published online November 20, 2020

**Abstract:** Electrochromism, an emerging energy conversion technology, has attracted immense interest due to its various applications including bistable displays, optical filters, variable optical attenuators, optical switches, and energy-efficient smart windows. Currently, the major drawback for the development of electrochromism is the slow switching speed, especially in inorganic electrochromic materials. The slow switching speed is mainly attributed to slow reaction kinetics of the dense inorganic electrochromic films. As such, an efficient design of nanostructured electrochromic materials is a key strategy to attain a rapid switching speed for their real-world applications. In this review article, we summarize the classifications of electrochromic materials, including inorganic materials (e.g., transition metal oxides, Prussian blue, and polyoxometalates), organic materials (e.g., polymers, covalent organic frameworks, and viologens), inorganic-organic hybrids, and plasmonic materials. We also discuss the electrochromic properties and synthesis methods for various nanostructured inorganic electrochromic materials depending on structure/morphology engineering, doping techniques, and crystal phase design. Finally, we outline the major challenges to be solved and discuss the outlooks and our perspectives for the development of high-performance nanostructured electrochromic materials.

**Keywords:** electrochromism; nanostructures; optical materials; plasmonics.

**\*Corresponding authors: Haizeng Li and Abdulkhakem Y. Elezzabi,** Department of Electrical and Computer Engineering, Ultrafast Optics and Nanophotonics Laboratory, University of Alberta, Edmonton, Alberta, T6G 2V4, Canada, E-mail: haizeng@ualberta.ca (H. Li), elezzabi@ualberta.ca (A. Y. Elezzabi). <https://orcid.org/0000-0002-8180-2800> (H. Li)

**Wu Zhang and Eric Hopmann,** Department of Electrical and Computer Engineering, Ultrafast Optics and Nanophotonics Laboratory, University of Alberta, Edmonton, Alberta, T6G 2V4, Canada, E-mail: wzhang1@ualberta.ca (W. Zhang), Hopmann@ualberta.ca (E. Hopmann). <https://orcid.org/0000-0002-9630-0977> (W. Zhang)

## 1 Introduction

Electrochromism is the phenomenon where the optical transmittance or absorbance of a material changes under an applied electric potential [1]. When a voltage is applied to an electrochromic material, the optical properties of the material are altered in a reversible fashion. Owing to the optical switching behavior, electrochromic materials provide great opportunities for a variety of energy-saving and color-tuning applications, including smart windows, multicolor bistable displays, and color-tunable optical elements [2–8].

Generally, electrochromic materials can be either organic or inorganic materials [9]. Among the organic electrochromic materials, organic molecules [10], polymers [11–13], and covalent organic frameworks [14] are widely investigated. These classes of organic electrochromic materials are characterized by their rich color palette, fast response, and ease of fabrication via solution-processing [15]. However, in comparison with the inorganic electrochromic counterparts, the organic electrochromic materials exhibit inferior thermal and chemical stabilities [16, 17], thus limiting their practical use. Recently, inorganic electrochromic materials have emerged at the forefront for real-world applications and potential commercialization. This class of materials offers key advantages, such as long-term durability, wide range of working temperature, and good chemical stability [18–20]. However, despite these advantages, they suffer from the shortcoming of poor switching speed [21, 22]. This is due to the low electrical conductivity of the inorganic material, the high-volume expansion during cycling, and the slow ionic transporting efficiency within the bulk material [23–25]. Reducing the size of the material is regarded to be an efficient strategy to enhance the dynamics of the inorganic material's response and improve its switching dynamics.

In recent years, nanostructured electrochromic materials have been investigated as a means to improve the switching speed because the nanostructured surface provides numerous active sites and shortens the ion's diffusion paths [26]. Moreover, the volume expansion of nanostructured electrochromic materials during the switching process is insignificant as the numerous surface

active sites increase the capacitive contribution during the redox reactions [27]. In other words, the ionic diffusion pathways inside the nanostructured materials are greatly shortened, which, in turn, improve the electrical conductivity [28]. Within this context, a nanostructured electrochromic material is expected to attain a rapid switching speed.

Although many literature reviews focus more on multifunctional electrochromic devices [29–33], a comprehensive review of recent achievements on nanostructured electrochromic materials is still lacking. In this article, we systematically discuss recent progress on designing nanostructured inorganic materials for high-performance electrochromic applications. This article first introduces the general classification of electrochromic materials and the key metrics used in evaluating electrochromic properties. This is followed by in-depth design strategies of nanostructured inorganic electrochromic materials and correlations between the electrochromic properties and synthetic methods for different nanostructured electrochromic materials. Next, the article highlights the challenges that need to be addressed in the future design of photonic devices. Finally, the authors' perspective and outlook to stimulate the development of electrochromic technology are presented.

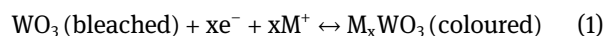
## 2 Classification of electrochromic materials

As the core component in an electrochromic device, electrochromic materials, having different optical properties, have been utilized for various electrochromic applications. Correspondingly, the electrochromic materials can be classified into a variety of types, including inorganic electrochromic materials, organic electrochromic materials, inorganic-organic hybrids, and plasmonic materials.



### 2.1 Inorganic electrochromic materials

Inorganic electrochromic materials mainly consist of the oxides of transition metals, which exhibit several different valence states on reduction. Electron delocalization between the mixed-valence states results in different bandgaps of inorganic materials, thus leading to different absorption of the light and inducing distinct color changes of the material [34]. There are two principally different types of electrochromic transition metal oxides which are classified in accordance with the coloration mechanisms: cathodic electrochromic materials, which are colored under guest ion insertion (reduction process); and anodic electrochromic materials, which are colored under guest cation extraction (oxidation process) [33]. The transition metals whose oxides possessing electrochromic properties are shown in the periodic table of elements (Figure 1).

As can be inferred from Figure 1,  $\text{WO}_3$ ,  $\text{TiO}_2$ ,  $\text{Nb}_2\text{O}_5$ ,  $\text{MoO}_3$ , and  $\text{Ta}_2\text{O}_5$  exhibit the cathodic coloration effect, which means that these oxides can be tinted via a reduction or cation intercalation [36–41]. These oxides commonly consist of highly distorted  $\text{MO}_6$  octahedra crystalline structure [42, 43], where M represents the transition metal atom. The layered structure, formed by the edge- and corner-sharing  $\text{MO}_6$  octahedra, facilitates ion transport through the conduits or chains of interstitial sites [44]. Notably, these oxides exhibit similar electronic band structures. Their intrinsically empty *d*-bands become populated on cathodic charge injection, and thus cause a color change through new intraband transitions [45, 46]. Among this class of oxides,  $\text{WO}_3$  is the most widely studied cathodic electrochromic material, especially used for electrochromic smart windows platforms. The  $\text{WO}_3$  layer is transparent in the oxidation state, whereas it can be tinted to blue as cations injected into the  $\text{WO}_3$  structures via the following reaction:



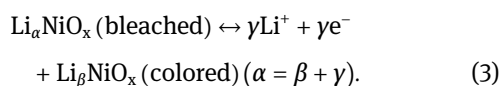
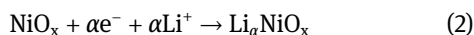
ELECTROCHROMIC OXIDES:

H		 Cathodic coloration  Anodic coloration																	He
Li	Be												B	C	N	O	F	Ne	
Na	Mg												Al	Si	P	S	Cl	Ar	
K	Ca	Sc	Ti	V	Cr	Mn	Fe	Co	Ni	Cu	Zn	Ga	Ge	As	Se	Br	Kr		
Rb	Sr	Y	Zr	Nb	Mo	Tc	Ru	Rh	Pd	Ag	Cd	In	Sn	Sb	Te	I	Xe		
Cs	Ba	La	Hf	Ta	W	Re	Os	Ir	Pt	Au	Hg	Tl	Pb	Bi	Po	At	Rn		
Fr	Ra	Ac																	

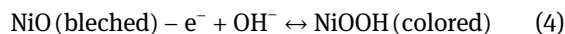
**Figure 1:** Electrochromic transition metal oxides showing both cathodic and anodic coloration. Reproduced with permission from Ref. [35]. Copyright 2017, Elsevier Ltd.

where  $M^+$  can be either  $H^+$  or an alkali metal ion, such as  $Li^+$ ,  $Na^+$ ,  $K^+$ ,  $Al^{3+}$ , or the recently reported  $Zn^{2+}$  [3]. Compared with used monovalent ions (e.g.,  $H^+$ ,  $Li^+$ ,  $K^+$  and  $Na^+$ ), multivalent ions (e.g.,  $Mg^{2+}$ ,  $Al^{3+}$ ,  $Zn^{2+}$ ) are expected to provide multiple charges to accelerate the redox reactions for fast electrochromic switching times [47, 48]. Another key advantage of multivalent ions, especially the  $Zn^{2+}$ , is their compatibility with aqueous electrolytes, which facilitates the formation of newly developed Zn-based electrochromic devices [2].

On the other hand, the anodic coloration effect is observed in  $NiO$ ,  $IrO_2$ ,  $Cr_2O_5$ ,  $MnO_2$ ,  $FeO_2$ , and  $Co_3O_4$  [49–55]. Such anodic electrochromic oxides usually serve as a counter electrode which is often used in conjunction with a cathodic electrochromic electrode in a complementary device [56, 57]. The most widely studied anodic electrochromic material is  $NiO$ , which is transparent in its reduced state and colors gray in its oxidized state [58]. The schematic reaction of  $NiO_x$  cycled in the  $Li^+$ -ion electrolytes can be summarized as follows [59, 60]:



The irreversible reaction (i.e., Eq. 2) refers to an activation process in the initial cycling of  $NiO_x$ . The reversible reaction, represented by Eq. (3), indicates the color switching processes accompanying the ion insertion/extraction. The insertion/extraction of  $OH^-$  can also lead to the oxidation/reduction of nickel oxide owing to the transformation of nickel ions between  $Ni^{2+}$  and  $Ni^{3+}$  [61]. This process can be summarized as follows [62]:



In addition to the aforementioned cathodic and anodic electrochromic materials, vanadium oxides (e.g.,  $V_2O_3$ ,  $V_3O_7$ , and  $V_2O_5$ ) are considered to be a type of bifunctional electrochromic material. This is due to their multicolor change properties under both anodically and cathodically potentials [63].

Along with the aforementioned transition metal oxides, Prussian blue (PB), represented as  $(Fe_4[Fe(CN)_6]_3 \cdot nH_2O)$  and its analogs (e.g.,  $KFe[Fe(CN)_6]$  and  $Na_2Fe[Fe(CN)_6]$ ) is another important type of inorganic electrochromic material. PB is a type of polynuclear transition metal hexacyanometallates. Similar to the anodic electrochromic transition metal oxides, PB exhibits a blue color in its oxidized state and can be reduced to Prussian white (colorless) via electrochemical redox reactions [64–67].

Recent investigations of PB-based electrochromic devices focused on the Zn-PB electrochromic devices because they show excellent energy retrieval functionalities [68–70]. Here, a Zn anode was used to reduce PB in a  $K^+$ - $Zn^{2+}$  dual-ion electrolyte and the constructed device was capable of self-bleaching via lighting an LED. Kang et al. deposited quasi-cubic PB particles with diameters of  $\approx 450$  nm on top of a fluorine-doped tin oxide (FTO)-coated glass substrate (Figure 2A) [68]. The Zn-PB electrochromic device achieved a high optical modulation of 84.9% at 633 nm during the voltage variation from 1.9 to 0.5 V (Figure 2B and C). This Zn-PB device also exhibited excellent cycling stability for up to 2000 cycles. Another example of the Zn-PB electrochromic device was recently reported by Li and Elezzabi [69]. Figure 2D and E depict an ideal unit cell of PB with guest ions and the working principle of Zn-PB electrochromic device. The Zn-PB electrochromic device exhibited an optical contrast of 78.6% between coloration/bleaching states (Figure 2F). Moreover, the Zn-PB electrochromic device possessed an open-circuit potential of 1.46 V (Figure 2F, inset) in the fully charged state, thus enabling self-bleaching behavior when lighting an LED. This open-circuit potential arises from the redox potential difference between the Zn foil and the PB electrode, thus providing the driving force that activates the oxidation of Zn and the reduction of the PB film. The built-in voltage allows the device to switch its color from blue to transparent while powering an LED for more than 60 min (Figure 2G). The feature of PB that stands out, in comparison with transition metal oxide-based electrochromic materials, is its fast color response that resulting from the PB's open framework structures [71, 72].

Another class of electrochromic materials that attracts recent attention are based on MXene. MXenes represent a large family of 2D transition metal carbides and nitrides which have been utilized for energy storage and various optoelectronic applications [73]. For example, titanium carbide ( $Ti_3C_2T_x$ ) has been shown to exhibit electrochromic properties cycling in 1 M phosphoric acid polyvinyl alcohol gel electrolyte ( $H_3PO_4$ /PVA gel) [74].

## 2.2 Organic materials

Electrochromic characteristics are shown by a wide range of organic materials, including organic molecules [75–77] and conjugated polymers [78–87]. Typically, organic electrochromic materials offer multiple colors under different applied biases, which are highly desired



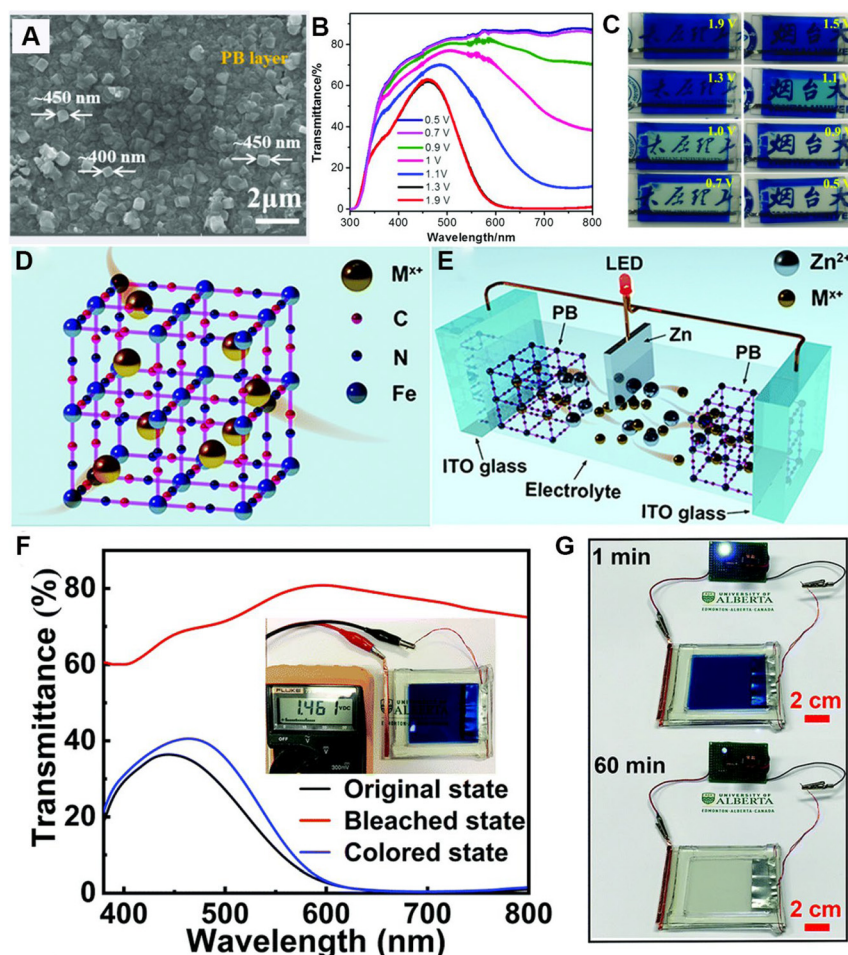


**Figure 2:** Structure, working principle, and application of Zn-PB electrochromic device. (A) Scanning electron microscope (SEM) image of the PB thin films. (B) Transmittance spectra of the Zn-PB device at different discharge voltages from 0.5 to 1.9 V. (C) Photographs of the Zn-PB electrochromic device at different discharge voltages. (A–C) Reproduced with permission from Ref. [68]. Copyright 2020, Wiley. (D) A schematic diagram of an ideal PB unit cell.  $M^{+}$  represents guest cations (e.g.,  $Li^{+}$ ,  $Zn^{2+}$ ,  $K^{+}$ ,  $Al^{3+}$ ,  $Na^{+}$  and the corresponding hydrated ions). (E) A schematic of the working principle of the Zn-PB electrochromic device. (F) Visible-near infrared transmittance spectrum of the Zn-PB electrochromic device under different states. The inset shows the open-circuit voltage (OCV) of the device. (G) Photographs of a 0.5 V LED powered by the Zn-PB electrochromic device along with an obvious self-bleaching phenomenon. (D–G) Reproduced with permission from Ref. [69]. Copyright 2020, Royal Society of Chemistry.

for multicolor displays. Viologens, 1,1'-disubstituted-4,4'-bipyridinium salts, are by far the most intensively investigated small molecule-based electrochromic materials [75]. Viologens exhibit three reversible redox states: a dication ( $V^{2+}$ ), a radical cation ( $V^{+}$ ), and a neutral form ( $V$ ), thus yielding differently colored species (Figure 3A). The intense color is produced upon reduction of the viologen dication, leading to a strong absorption at its radical cation state. The substitution groups on the nitrogen of the bipyridinium salt mainly control the colors of their reduction states. As illustrated in Figure 3B, an ethyl viologen-based electrochromic device exhibits a blue color in its reduced state and a light yellow color in its oxidized state [77]. The major advantages of viologens as electrochromic materials reside in their high optical contrast, excellent coloration efficiency (CE), ease in molecular design, and the feasibility for large-area assembly. A successful application is their use by Gentex Corporation as a smart window in Boeing 787 aircraft [30].

Some long-chain polymers, such as polypyrroles [78–80], polythiophenes [81–83], and polyanilines [85, 86], are found to possess electrochromic properties by altering the structures of their  $\pi$ -conjugated systems. Polyaniline (PANI) films exhibit reversible multicolors: transparent  $\leftrightarrow$  pale yellow  $\leftrightarrow$  green  $\leftrightarrow$  blue, as the applied potential is varied [88]. As shown in Figure 3C, PANI films can be prepared on flexible indium tin oxide (ITO)/polyethylene terephthalate substrates [86]. The optical transmission spectra of PANI films at different potentials and color states are shown in Figure 3D. The transmittance variation between colorless and blue states can be as high as 49% at 630 nm as the applied potential increased from  $-0.2$  to  $1.0$  V. Another interesting polymer is poly(3,4-ethylenedioxythiophene) polystyrene sulfonate (abbreviated as PEDOT:PSS). PEDOT:PSS is a conductive polymer which exhibits a blue coloration on electrochemical reduction. Figure 3E depicts a series of images of the electrochromic symmetrical displays built from PEDOT:PSS films of various thickness [84]. A clear color gradient was observed with the increase of thickness in reduced (colored) state as

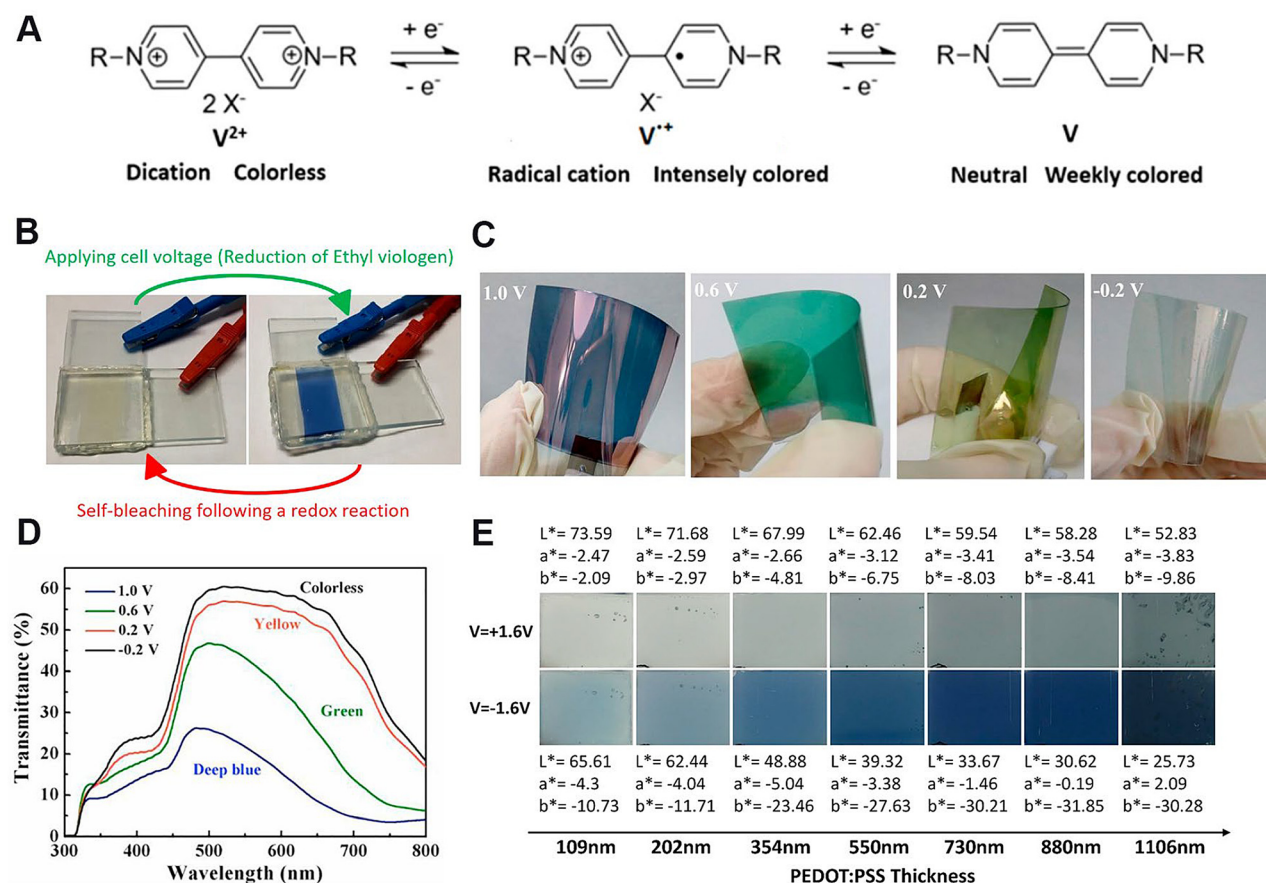


**Figure 3:** Characterization and demonstration of organic electrochromic materials.

(A) Different redox states of viologen. (B) The photographs of ethyl viologen-based electrochromic device at bleached and colored states. (A–B) Reproduced with permission from Ref. [75]. Copyright 2019, Multidisciplinary Digital Publishing Institute. (C) The photographs of the flexible polyaniline (PANI) film electrode in its colored state at the different potentials. (D) The corresponding optical transmittance spectra of the flexible PANI film electrode at different potentials. (C–D) Reproduced with permission from Ref. [86]. Copyright 2018, Elsevier Ltd. (E) Photographs of the electrochromic symmetrical displays built from PEDOT: PSS films with different thicknesses, showing an oxidized state for a potential of +1.6 V and a reduced (colored) state for a potential of –1.6 V. The corresponding measured CIE  $L^*a^*b^*$  parameters are labeled. Reproduced with permission from Ref. [84]. Copyright 2019, Multidisciplinary Digital Publishing Institute.

distinguished by the CIE  $L^*a^*b^*$  color space parameters. Clearly, utilizing PEDOT:PSS as a transparent conducting electrode is promising in applications requiring a stretchable electrochromic platform [89, 90].

### 2.3 Inorganic–organic hybrids

Different electrochromic materials have their respective advantages and disadvantages, thus instead of using a single class of electrochromic materials, organic–inorganic electrochromic hybrids can combine the advantages of each platform, thus offering enhanced electrochromic properties. Considerable efforts have been devoted toward the development of organic–inorganic electrochromic nanocomposites, wherein the assembly of the organic

polymers into an inorganic porous framework is shown to lead to enhanced electrochromic performance and chemical stability [91–93]. For example, the organic polymers PEDOT:PSS can also be introduced into porous nanorod layers of tungsten molybdenum oxide ( $W_{0.71}Mo_{0.29}O_3$ ) [92]. Figure 4A and B schematically illustrate the spray layer-by-layer assembly process used to prepare the  $W_{0.71}Mo_{0.29}O_3$ /PEDOT:PSS hybrid electrochromic films. The PEDOT:PSS chains were observed to permeate into the porous nanorod layers of the  $W_{0.71}Mo_{0.29}O_3$ , forming an interconnected conductive network (Figure 4C and D). The  $W_{0.71}Mo_{0.29}O_3$ /PEDOT:PSS hybrid electrochromic films realized an improved electrochromic performance that is superior to both pure PEDOT:PSS and  $W_{0.71}Mo_{0.29}O_3$  films. In the organic–inorganic nanocomposites, the interfacial interactions between the organic and the inorganic phases



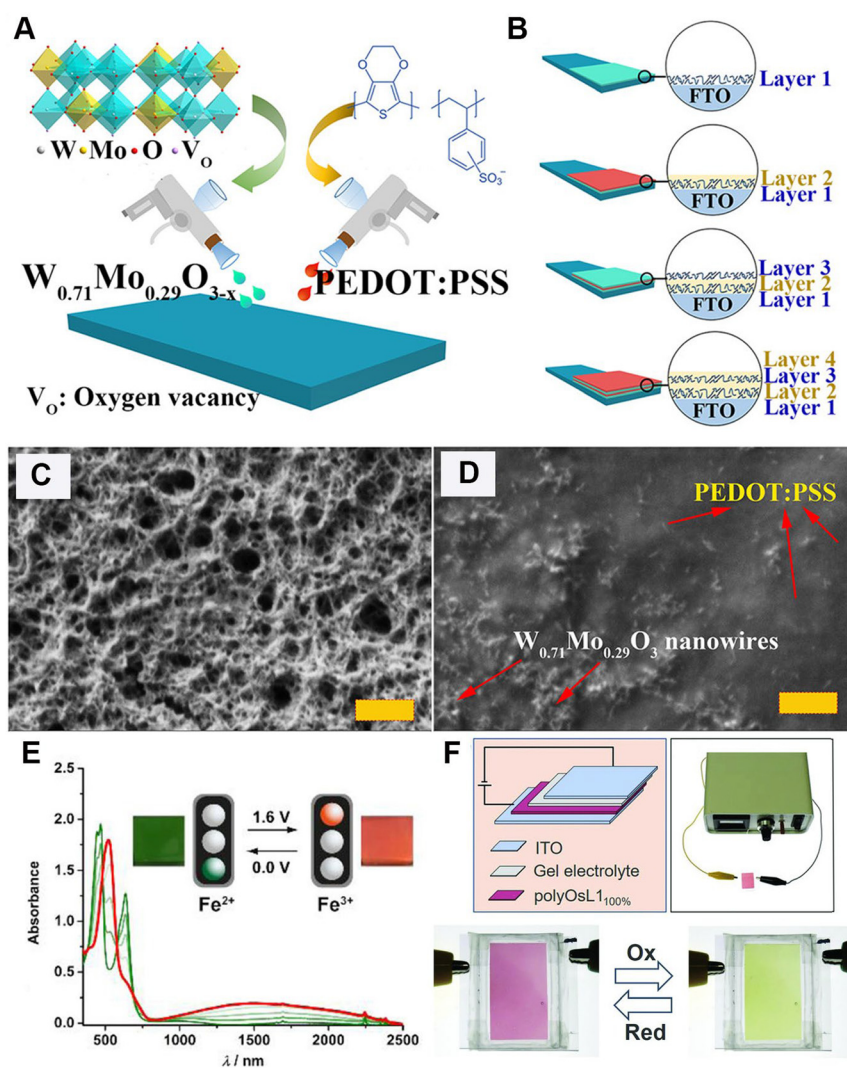


**Figure 4:** Preparation and characterization of organic-inorganic hybrid films.

(A) Schematic illustration of the spray layer-by-layer assembly process used to prepare the  $W_{0.71}Mo_{0.29}O_3$ /PEDOT:PSS hybrid electrochromic films. (B) Schematic illustration of the evolution of the  $W_{0.71}Mo_{0.29}O_3$ /PEDOT:PSS hybrid electrochromic films during the initial four cycles. Layers 1 and 3 depict the porous structure of  $W_{0.71}Mo_{0.29}O_3$  material, whereas Layers 2 and 4 depict the PEDOT:PSS material. (C) Field emission scanning electron microscope (FESEM) image of the spray-coated pure  $W_{0.71}Mo_{0.29}O_3$  films (D) FESEM image of the spray-coated  $W_{0.71}Mo_{0.29}O_3$ /PEDOT:PSS hybrid films (A–D) Reproduced with permission from Ref. [92]. Copyright 2018, American Chemical Society. (E) Optical absorbance of FeL2-MEPes at different potentials with the corresponding photographs of the thin films. Reproduced with permission from Ref. [104]. Copyright 2017, American Chemical Society. (F) Schematic illustration of linear  $Os^{II}$ -based MEPes electrochromic device. Reproduced with permission from Ref. [105]. Copyright 2018, Wiley.

have a large impact on the properties of the nanocomposites. A good distribution of the introduced materials within the matrix material and their strong interfacial interaction is shown to improve the mechanical and electrochromic properties of structural nanocomposites because of the synergic effect of these materials [94, 95]. A recent study demonstrated a class of hybrid electrochromic materials utilizing polythiophenes and tin-doped indium oxide nanoparticles that enabled the independently modulating visible and near-infrared light [96]. This inorganic–organic hybrid electrochromic film combines polythiophenes to modulate visible light with tin-doped indium oxide nanoparticles that modulate near-infrared light. Therefore, such hybrid materials can be operated in three distinct voltage regimes, each of which uniquely modulates visible and near-infrared light. Besides simple physical contact, the strong interfacial interactions between the organic and inorganic components (e.g., covalent bond, coordination

bond, electrostatic interaction, hydrogen bond, and  $\pi$ – $\pi$  stacking interaction) are conducive for avoiding structural damage caused by the volume change during the switching process and thus improving the structural stability of the hybrids [97–100]. For example, Yang et al. studied covalently bonded  $WO_3$ /polyvinylimidazole core–shell microspheres [98]. It is found that the chemical and thermal stabilities of covalently bonded  $WO_3$ /polyvinylimidazole are higher than those of pure  $WO_3$  nanoparticles and noncovalently bonded  $WO_3$ /polyvinylimidazole. The covalent bond ( $\sim 100$  to  $500 \text{ kJ mol}^{-1}$ ) can supply solid strength for the organic/inorganic electrochromic nanocomposites, leading to enhanced electrochemical and electrochromic performances [97].

Another important example of inorganic–organic hybrids is metallo-supramolecular polyelectrolytes (MEPEs). This hybrid electrochromic material is based on the metal-to-ligand charge transfer and the intervalence charge transfer [101–103]. Through altering the metal ion center or

the surrounding organic ligands, MEPE can switch between various colors. As shown in Figure 4E, Kurth et al. reported a reversible redox behavior of  $\text{Fe}^{\text{II}}/\text{Fe}^{\text{III}}$  in FeL2-MEPes device where a color-switching between the red and the green colors was demonstrated [104]. Furthermore, electrochromic performance can be observed in  $\text{Os}^{\text{II}}$ -based MEPes [105]. Figure 4F illustrates an electrochromic device using linear  $\text{Os}^{\text{II}}$ -based MEPes, where a distinct color change from yellow-green to pale-pink was observed on reduction reaction.

## 2.4 Nanoparticles and nanostructured plasmonic material

Plasmonic devices can experience an unconventional electrochromic process, where the color modulation of the electrochromic device is primarily based on dynamically changing the resonance of plasmonic nanostructures. Nanoparticles plasmonic materials are identified as either colloidal metal nanoparticles, which allow for reversible metal deposition, or highly doped metal oxide nanocrystals that can be electrochemically charged in a capacitive manner due to their extremely small size and high surface area [45]. Light couples to the colloidal plasmonic material via the resonant excitation of free charge carriers as localized surface plasmon resonances (LSPRs). Here, LSPR enables a wide range of spectral tunability by changing the nanocrystal size, altering the host environment, or via doping or injection of charges. When the incident electromagnetic radiation frequency matches the natural resonance frequency of collective electron oscillations in the conduction band (or holes in the valence band) of the nanocrystals (Figure 5A), light absorption and scattering of nanocrystals are notably enhanced. Although the LSPR frequency of nanocrystals is slightly tunable by their shapes, the doping level, and the nanostructure size, the free electron density plays a key role because it determines the starting position, width, and intensity of the LSPR absorption peak [106–108]. Typically, metal-based plasmonic nanostructures exhibit intrinsic free carrier density on an order of  $10^{22} \text{ cm}^{-3}$  [109], which leads to high energy electronic oscillations resulting in plasmonic resonance frequencies in the visible spectral range. Metal-based electrochromic devices have been demonstrated via reversible electrochemical deposition. Although metals lack the oxidation states necessary for an inherent electrochromism, unconventional electrochromic devices have been demonstrated through the deposition of Ag nanoparticles on an ITO electrode [110–112]. Here, the redox reaction occurs when  $\text{Ag}^+$ -ions

are reduced at the electrode and thereby agglomerate into elemental metal nanoparticles. Oppositely, an inverse charge can lead to the dissolution of Ag nanoparticles. As such, the deposition and dissolution of Ag nanoparticles are reversible, and thus leading to the reversible optical evolution. Based on the size and shape of the deposited particles, which are strongly dependent on the deposition time, bias voltage, and chemical makeup of the solvent, the resonance frequency can be modulated over a wide range. A recent study by Kobayashi et al. demonstrated a multicolor electrochromic device based on the Ag deposition mechanism [111]. Figure 5B illustrates the morphology of Ag deposited on the ITO particle-modified electrode having a diameter size of 21 nm. With the deposition of Ag on the ITO electrode, the LSPRs of Ag nanoparticles result in displaying multicolors (Figure 5C).

Highly doped metal oxide nanocrystals exhibit charge carrier densities in the range of  $10^{20}$ – $10^{22} \text{ cm}^{-3}$ , which leads to pronounced surface plasmon resonances in the near-infrared spectral range. The resonance of free carriers can be modulated through an electrochemical gating process [113]. The change in carrier concentration leads to a shift in the LSPR frequency and a change in absorption, giving rise to plasmonic electrochromism [45]. Even though this plasmonic electrochromism does not lead to a change in the oxidation state of the material, devices based on metal oxide plasmonic nanostructures show reversible optical transmission changes through electrochemical charge modulation. Figure 5D depicts an illustration of the capacitive nature of the plasmonic electrochromic mechanism. The modulation of the electron/hole density is electrochemically controlled by the application of negative and positive potentials to the material. Milliron et al. demonstrated a surface plasmon effect in tin-doped indium oxide (ITO) nanocrystalline film [114]. Figure 5E illustrates a transmission electron microscopy (TEM) image of the ITO nanocrystals having varying sizes of  $4.1 \pm 0.6 \text{ nm}$ . When different potentials are applied, the surface plasmon resonance peak of the ITO nanocrystalline film (4.1 nm diameter, 16.8% Sn) was shown to be enhanced and shifts to higher energy (Figure 5F).

In addition, conventional electrochromic materials, such as tungsten oxide or polyaniline, can be used to modulate the LSPR frequency of metallic plasmonic nanostructures. Chumanov et al. utilized a  $\text{WO}_3$ -sol on an array of Ag nanoparticles to reversibly modulate the resonance frequency of the Ag particles by changing their dielectric surroundings [115]. Recently, several studies have shown the potential of electrochromic modulation of the dielectric environment of metallic nanostructures for a

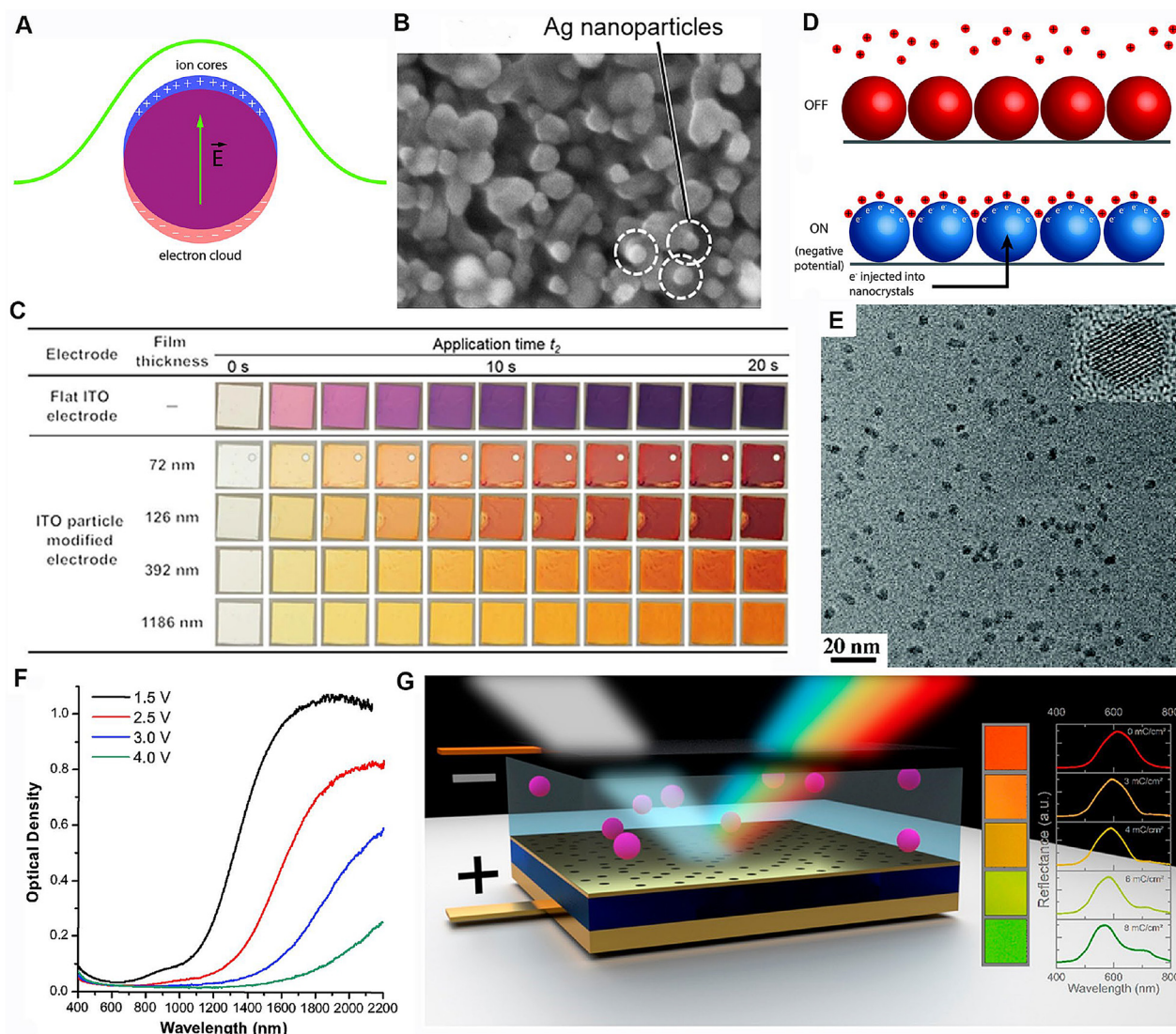


**Figure 5:** Depiction of plasmonic electrochromic nanocrystals and nanostructures.

(A) Illustration of a localized surface plasmon in a nanocrystal. Incident electromagnetic radiation displaces the free electron cloud, which then experiences a restoring force exerted by the positively charged ion cores. Reproduced with permission from Ref. [45]. Copyright 2014, Royal Society of Chemistry. (B) Scanning electron microscope (SEM) image of the Ag nanoparticles deposited on the ITO particle-modified electrode. (C) Photographs of the working electrodes with various ITO film thicknesses during the Ag deposition process. (B–C) Reproduced with permission from Ref. [111]. Copyright 2014, American Chemical Society. (D) The mechanism of capacitive electrochromism based on nanocrystal films. In the OFF state, a positive potential is applied to the nanocrystals, no electrons and ions gather at the surface of nanocrystals. In the ON state, a negative potential is applied to the nanocrystals, ions are absorbed to the surface of nanocrystals in order to neutralize the injected electrons. Reproduced with permission from Ref. [45]. Copyright 2014, Royal Society of Chemistry. (E) TEM image of ITO nanocrystals. (F) Potentials-dependent optical density of a film composed of 4.1 nm diameter, 16.8% Sn ITO nanocrystals. (E–F) Reproduced with permission from Ref. [114]. Copyright 2011, American Chemical Society. (G) Schematic of a plasmochromic device based on an electrochromic  $\text{WO}_3$  layer and a gold resonator. Reproduced with permission from Ref. [118]. Copyright 2020, American Chemical Society.

full-color generation [116–118]. In general, these devices make use of the inherent change of the refractive index of an electrochromic material during the intercalation and the deintercalation processes. This change is utilized to shift the resonance frequency of plasmonic nanostructures, such as colloids and nanohole arrays. Hopmann and

Elezzabi reported a plasmonic metal-insulator–nanohole cavity based on an electrochromic  $\text{WO}_3$  insulator layer. Through intercalation and deintercalation of lithium ions ( $\text{Li}^+$ ) into the  $\text{WO}_3$  film, a broad peak resonance wavelength shift of 64 nm was realized, leading to distinct color reflection (Figure 5G) [118].



### 3 Key metrics for electrochromic materials

An electrochromic material alters its optical and electrical properties in response to an external voltage bias. A high-performance electrochromic material must possess fast color switching, reversible light modulations, high color contrast, low energy consumption, and long-term chemical and thermal stabilities. Key performance metrics are introduced and highlighted below.

#### 3.1 Color and optical contrast

Color is an important aspect in assessing the performance of electrochromic materials as their applications rely on switching between different colors. The colorimetric analysis is usually performed based on the protocols set out by the International Commission on Illumination (CIE). The CIE 1931 xyY color space is widely used to specify color in practice. As shown in Figure 6A, an electrochromic film configured in ultracompact Fabry–Perot nanocavities displays seven distinguished colors [17]. The Fabry–Perot nanocavities utilize partially reflective tungsten metal as the current collector and the reflector layer. As the thickness of the  $\text{WO}_3$  thin film changes, various structural colors are generated. These colors cause a remarkable shift of the CIE color coordinates (Figure 6B), forming a circular area with different tints. More interestingly, the Fabry–Perot nanocavity-type electrochromic films exhibit a large variety of multicolor states under different applied potentials (Figure 6C). Although the 163-nm-thick  $\text{WO}_3/\text{W}$  electrode produces a gradual color change from red to green at different biases (Figure 6D), the reflection spectrum displays a drastic shift from 760 to 517 nm in its peak position (Figure 6E).

The intensity difference between the colors is an important factor in determining the quality of the electrochromic coloration process. As such, the optical contrast, referring to the degree of optical change during the switching process (intensity change in transmittance  $[\Delta T \ %]$ , absorbance  $[\Delta A \ %]$  or reflectance  $[\Delta R \ %]$ ), is another metric used in evaluating the electrochromic material performance. However, when describing the optical contrast of electrochromic materials or devices, it is customary to report this parameter at a single wavelength. This wavelength is selected to be either the wavelength at which a maximum absorbance occurs or the wavelength of maximum human visual sensitivity (i.e., 550 nm) [44]. Figure 6F depicts a  $\text{WO}_3$ -based electrochromic device, where a 63% change in transmittance

at 633 nm was achieved at an applied voltage of  $-2.5 \text{ V}$  [22]. The choice of the 633 nm wavelength used to calculate the optical contrast is dictated by the maximum absorbance observed at this wavelength. In general, the optical contrast of a material mainly depends on the thickness of the electrochromic layer [119]. As the film thickness increasing, the transmittance of both the colored and bleached states will decrease. Typically, the maximum optical contrast is reported at an attained intermediate thickness of a few hundred nanometers [120, 121]. The design of nanostructured electrochromic materials is expected to enhance the electrochromic performance (e.g., optical contrast, switching times, CE, and cycling stability) [122–124]. A recent study by Scherer et al. demonstrated that the gyroid-structured vanadium pentoxide films surpass previous inorganic electrochromic materials in all relevant parameters: the switching speed, coloration contrast, and composite CE [125].

#### 3.2 Coloring and bleaching switching times

Switching times, also known as the response times, refer to the times required to switch between the colored/bleached and the bleached/colored states of an electrochromic material or a device. The coloration and bleaching times are defined as the time required for 90% change in the entire optical modulation [126]. As a key parameter when considering the suitability of an electrochromic device for light modulation applications, fast switching between the different color states is highly desirable. Figure 7A illustrates an Al anode-based electrochromic energy storage smart window switching between 4 V (transparent state), 2.2 V (cool state), and 1.6 V (dark state) [4]. The switching times of this device were calculated to be 71 s for bleaching and 19 s for coloration at 633 nm, and 56 s for bleaching and 18 s for coloration at 1200 nm (Figure 7B and C). Generally, the switching times of an electrochromic layer will increase as the film thickness increasing. Thicker films with a fixed porosity would lead to longer ion-transport pathways to insert into the inner active materials, which results in longer switching times [127–129]. The nanostructured electrochromic materials with large surface active area are promising for fast switching times as the active materials are easy to access for guest ions [130, 131]. For example, rapid switching times of 0.5/0.9 s for the coloration and bleaching processes were reported for nanostructured electrochromic materials: core-shell halloysite nanotube (HNT)@inherently conducting polymer nanocomposites [130]. Other Parameters, such as the electrolyte properties, counter electrode material composition, substrate sheet resistance and device size, all have a significant effect on the switching times.

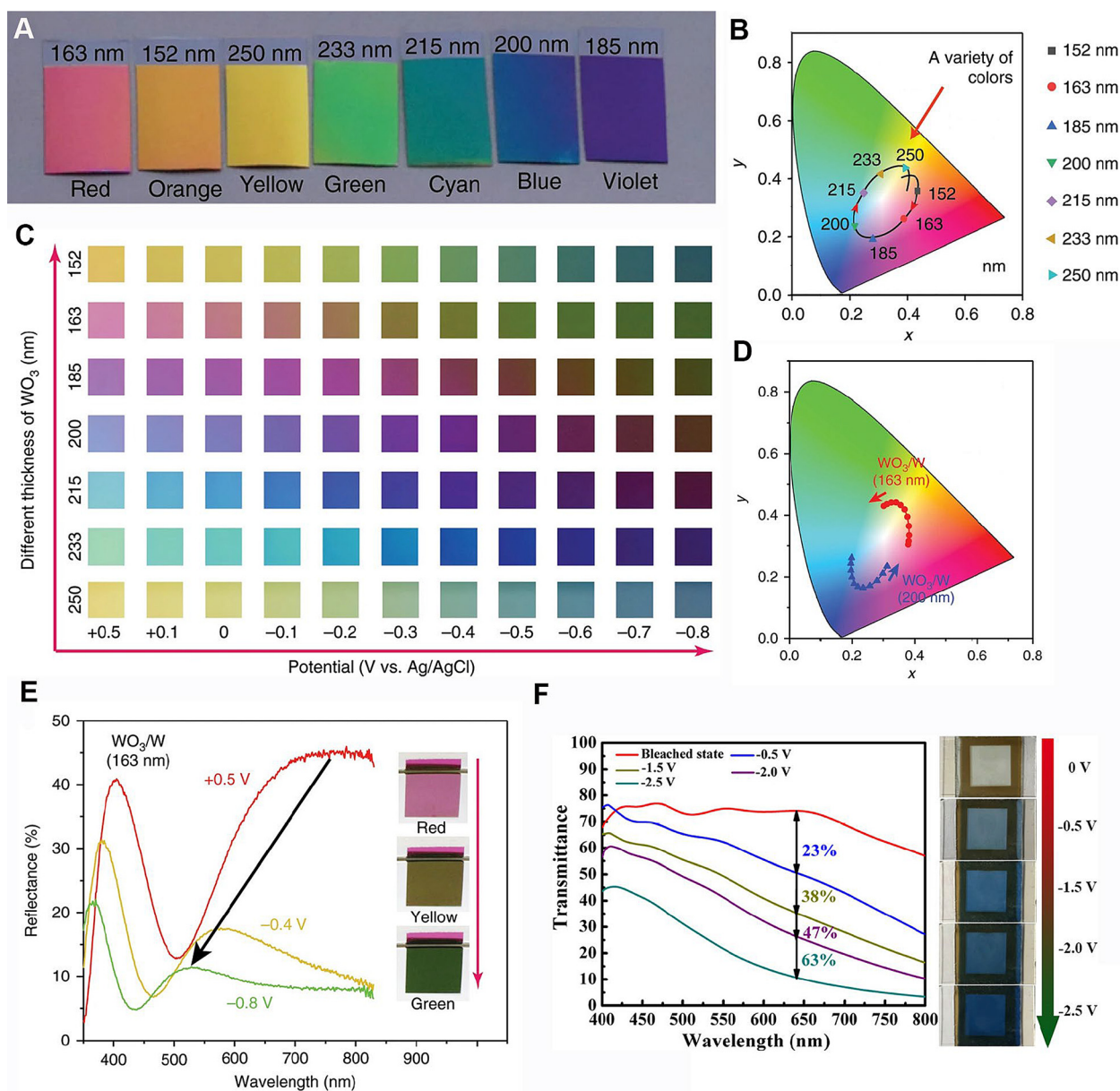


**Figure 6:** Demonstration of electrochromic materials having different colors and light spectra.

(A) Photographs of the  $\text{WO}_3/\text{W}$  electrodes having different thicknesses of the  $\text{WO}_3$  layer. (B) CIE color coordinates of the  $\text{WO}_3/\text{W}$  electrodes having different thicknesses of the  $\text{WO}_3$  layer. (C) Color gallery obtained from the  $\text{WO}_3/\text{W}$  electrodes under different voltage biases. (D) CIE color coordinates of the 163/200-nm-thick  $\text{WO}_3/\text{W}$  electrode under different voltage biases. (E) Reflectance spectra and photographs of the 163-nm-thick  $\text{WO}_3/\text{W}$  electrode under different voltage biases. (A–E) Reproduced with permission from Ref. [17]. Copyright 2020, Nature Publishing Group. (F) Transmittance spectra and photographs of  $\text{MoO}_{2+x}\text{-WO}_3$  electrochromic device. Reproduced with permission from Ref. [22]. Copyright 2019, American Chemical Society.

### 3.3 Coloration efficiency

An energy-efficient electrochromic material requires a high optical contrast while consuming fewer charges in the process. In this regard, CE, representing the change in optical density ( $\Delta\text{OD}$ ) per unit of charge intercalated into

the electrochromic layer, is proposed to evaluate the energy-related efficiency accordingly,

$$\Delta\text{OD} = \log(T_c/T_b) = \eta Q/A, \quad (4)$$

where  $\eta$  is CE,  $Q$  is the charge (C),  $A$  is the active area of the electrochromic material ( $\text{cm}^2$ ),  $T_c$  and  $T_b$  are the

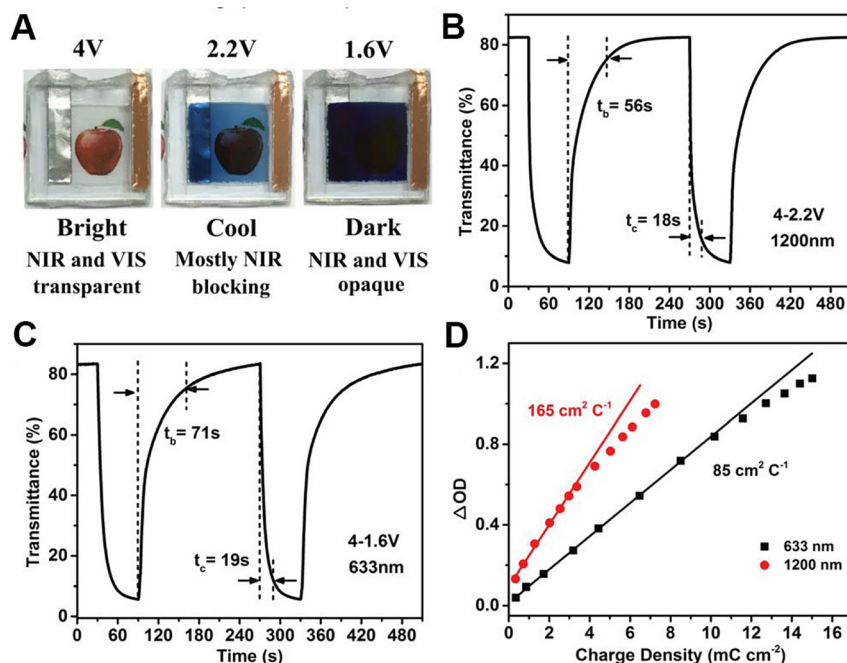


**Figure 7:** Al anode-based electrochromic energy storage windows.

(A) Photographs of an Al anode-based electrochromic energy storage window at different applied potentials. (B) The dynamic test of the device between 4 and 2.2 V at 1200 nm. (C) The dynamic test of the device between 4 and 1.6 V at 633 nm. (D) Coloration efficiency of the device switching at 633 and 1200 nm. (A–D) Reproduced with permission from Ref. [4]. Copyright 2019, Wiley.

transmittances of electrochromic devices at coloration and bleaching states, respectively. An example of CE value calculation is shown in Figure 7D. Here, the Al anode-based electrochromic energy storage window exhibited CE values of  $165 \text{ cm}^2 \text{ C}^{-1}$  at 1200 nm and  $85 \text{ cm}^2 \text{ C}^{-1}$  at 633 nm, respectively. The CE will increase as the thickness increasing till a maximum point, then the CE will decrease as the thickness keeps increasing [132, 133]. The maximum CE value is obtained at an intermediate thickness (~ a few hundred nanometers), which requires rational design and carefully screening several thicknesses of electrochromic films. This phenomenon probably relates to the different ionic/electric resistance of the electrochromic films at various thicknesses [134]. Because the CE is an intrinsic parameter of electrochromic materials and mainly relies on the morphology of the materials [135], the design of nanostructured electrochromic materials having large surface active area is required to achieve high CE values. As reported by Ma et al., the CE value of  $\text{WO}_3$  nanoflake films is much higher than the  $\text{WO}_3$  nanoparticle/nanorod films [136].

### 3.4 Cycling stability

Cycling stability is the loss of the optical contrast on electrochemical cycling and is another important parameter used to evaluate the long-term stability of the electrochromic device [137]. For practical applications,

electrochromic materials are expected to exhibit a cycle life of more than  $10^5$  cycles. However, in laboratory exploration, cycling stability is often reported for a small area of electrochromic film which is not sufficient for real-world applications. Both physical and chemical stabilities are crucial to the cycling stability of an electrochromic thin film. Generally, as the electrochromic film's thickness increasing, the electrochromic film would suffer a poor adhesion to the substrate and thus leading to the significant degradation of the cycle performance due to the peeling of active materials [138]. A strong interfacial interaction between the film and the substrate will certainly enhance the cycling stability [139]. The design of nanostructures is expected to improve both physical and chemical stability of thin films. Nanostructured electrochromic materials can be designed to optimize the contacting area between the film and the substrate and hence providing a strong interfacial adhesion [140]. In addition, the volume expansion of nanostructured electrochromic materials during the switching process is supposed to be significantly eliminated as the numerous surface active sites increase the capacitive contribution during the redox reactions [141]. In other words, nanostructured electrochromic materials possess excellent chemical stability on cycling. Besides the stability of thin films, the cycling stability of an electrochromic device is influenced by several factors, including the electrolyte properties, the counter electrode material, and the device dimensions.



## 4 Design of nanostructured inorganic electrochromic materials

To develop electrochromic materials having high performance, including the aforementioned metrics for potential real-world applications, a list of recent achievements on the fabrication of promising inorganic electrochromic materials is presented. It is hoped that universal strategies for fabricating nanostructured inorganic electrochromic materials can be realized to advance the future development of the electrochromism.

### 4.1 Tungsten oxides

The most commonly used cathodic electrochromic materials are based on tungsten oxides (e.g., tungsten oxide, hydrated tungsten oxide, and doped tungsten oxide). Naturally, bulk tungsten oxide exhibits intrinsic oxygen deficiencies [142], making the material appear yellowish. By contrast, in a thin-film configuration, stoichiometric tungsten oxide is transparent and becomes blue on applying a cathodic potential [143]. Tungsten oxide has a nearly cubic structure formed by  $\text{WO}_6$  octahedra that share corners [144]. The void space inside the cubes provides the accessibility of numerous interstitial sites where guest ions (e.g., protons or alkali cations) can be inserted. The first study on the electrochromic effect in tungsten trioxide was reported in 1969 [145]. Over the past decades, the most promising application of the  $\text{WO}_3$  electrochromic coating is as a switchable glazing for smart windows. The color change in  $\text{WO}_3$  electrochromic smart windows offers an important energy-efficient module for designing environmentally friendly buildings by reducing the cost of air conditioning, controlling direct sun illumination, and simultaneously improving the indoor living comfort for the occupants [25].

Recently, nanostructured  $\text{WO}_3$  films have been realized for practical applications because of their excellent electrochromic performance. A variety of crystallographic and morphological structures of  $\text{WO}_3$  films have been reported to exhibit shorter switching time, higher coloration efficiencies, and higher cycling stabilities compared with their bulk counterparts. The nanostructured  $\text{WO}_3$ , including nanoparticles [62, 146], nanowires [147], nanosheets [148], nanofibers [149], and hierarchical structures [150], possess a large interfacial contact area with the electrolyte, short ions diffusion pathway, and good structure stability associated with

the intercalation/deintercalation of guest ions. These advantages of nanostructured  $\text{WO}_3$  give rise to highly efficient and stable electrochromic performance. Shan et al. reported the first demonstration of tungsten oxide quantum dots (QDs) for electrochromic applications [151]. As shown in Figure 8A, because the QDs size is very small ( $\sim 1.6$  nm), this yielded a fast electron/ion transport during the coloration/bleaching process. Similarly, Yao et al. reported  $\text{WO}_3$  QDs with an average diameter of 1.2 nm (Figure 8B) [152]. The cycle stability of  $\text{WO}_3$  QDs electrochromic films can reach 20,000 cycles on the intercalation/deintercalation of  $\text{Al}^{3+}$ . Moreover, larger  $\text{WO}_3$  QD nanocrystals and their inks ( $\sim 4$  nm in diameter, Figure 8C and D) were investigated by Zhang et al. for inkjet-printed flexible electrochromic devices [146]. The printed tungsten oxide thin films are assembled into a novel Zn-based electrochromic pseudocapacitive device, which exhibits a relatively high capacity ( $\sim 260 \text{ C g}^{-1}$  at  $1 \text{ A g}^{-1}$ ). In addition to the aforementioned QD  $\text{WO}_3$  nanocrystalline structures, Zhang et al. reported oxygen-deficient monoclinic tungsten oxide nanowire ( $\text{m-WO}_{3-x}$  NW) (Figure 8E and F). With efficient  $\text{Al}^{3+}$  intercalation/deintercalation, the  $\text{m-WO}_{3-x}$  NWs-based electrochromic device delivered not only efficient and independent control of near-infrared and visible light transmittance but also exhibited high CE [47]. High optical contrast of 93.2%, high CE of  $121 \text{ cm}^2 \text{ C}^{-1}$ , fast switching times of 16/13 s, and good cycling stability (5.5% capacity loss after 2000 cycles) were reported. An interesting form of nanostructured  $\text{WO}_3$  films is the hierarchical nest-like  $\text{WO}_3 \cdot 0.33\text{H}_2\text{O}$  film (Figure 8G). Li et al. reported a self-seeded hydrothermal process that eliminates the grain boundaries existing in the nanocrystalline seed layer [153]. This process accelerates electron transport to the FTO glass substrate and promotes electron transfer efficiency. As shown in Figure 8H, the prepared  $\text{WO}_3 \cdot 0.33\text{H}_2\text{O}$  films have an optical contrast of 40.8 and 57.6% after applying voltages of  $-0.5$  and  $-1.0$  V, respectively. The response times of  $\text{WO}_3 \cdot 0.33\text{H}_2\text{O}$  films are found to be 26 and 5.5 s under  $\pm 3.0$  V bias. Owing to the large active surface area, this self-seeded film also exhibits a high CE value of  $126.34 \text{ cm}^2 \text{ C}^{-1}$ .

Doping  $\text{WO}_3$  with other elements has been realized as an efficient method to tune the nanostructures of  $\text{WO}_3$  [56]. Li et al. reported that the molybdenum doping of  $\text{WO}_3$  significantly reduces the particle size of the  $\text{WO}_3$ . The solution-based fabrication process was simple and inexpensive to allow for large-scale fabrication of electrochromic films [126]. Furthermore, a slight increase of the Ni content (from 0 to 2.5%) alters the surface morphology of the  $\text{WO}_3$  film (Figure 8I–L) [56]. For the undoped  $\text{WO}_3$  film (Figure 8I), the SEM image shows a porous network structure. Whereas by doping the film with only 0.5% Ni, the Ni- $\text{WO}_3$  grows into vertically aligned nanorod array

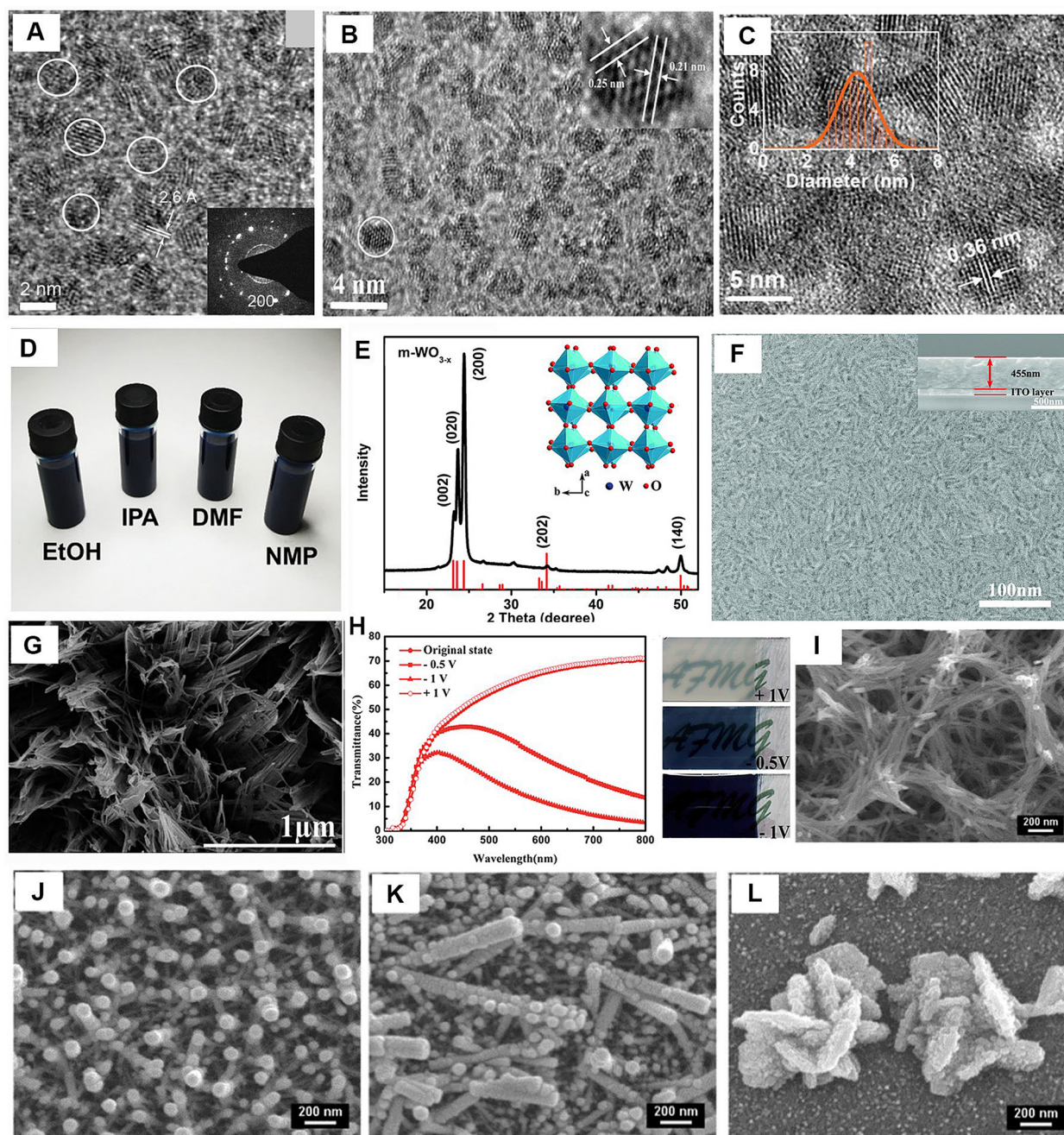


**Figure 8:** Structure and characterization of  $\text{WO}_3$ -based electrochromic films.

(A) Transmission electron microscopy (TEM) image of tungsten oxide quantum dots (QDs) with average sizes of 1.6 nm. Reproduced with permission from Ref. [151]. Copyright 2014, Wiley. (B) High-resolution TEM image of as-prepared tungsten oxide QDs. Reproduced with permission from Ref. [152]. Copyright 2020, Elsevier. (C) TEM image of  $\text{WO}_{3-x}$  nanocrystals. Inset shows the nanocrystals diameter statistics. (D)  $\text{WO}_{3-x}$  inks based on four different solvents. (C–D) Reproduced with permission from Ref. [146]. Copyright 2020, Wiley. (E) XRD patterns and crystal structure (inset) of  $\text{m-WO}_{3-x}$  NWs. (F) Surface and cross-sectional (inset) SEM images of  $\text{m-WO}_{3-x}$  NW films. (E–F) Reproduced with permission from Ref. [47]. Copyright 2018, Royal Society of Chemistry. (G) Scanning electron microscope (SEM) image of self-seeded grown  $\text{WO}_3 \cdot 0.33\text{H}_2\text{O}$  electrode with less amount of ethylene glycol. (H) Optical transmittance spectra and photographs of the self-seeded grown  $\text{WO}_3 \cdot 0.33\text{H}_2\text{O}$  film measured at different biases. (G–H) Reproduced with permission from Ref. [153]. Copyright 2014, Royal Society of Chemistry. FESEM images of  $\text{WO}_3$  films doped with different Ni content: (I) 0%, (J) 0.5%, (K) 1.5% and (L) 2.5%. (I–L) Reproduced with permission from Ref. [56]. Copyright 2016, Royal Society of Chemistry.

structures (Figure 8J). As the doping concentration of Ni is increased to 1.5%, the nanorods become randomly distributed nanorods (Figure 8K). Once the Ni doping content was increased to 2.5%, nanorods disappeared and nanoflowers composed of clusters of nanoplates appear (Figure 8L). For the  $\text{WO}_3$  films with 0–1.5% Ni doping, the electrochromic performance is found to be enhanced with the increase of Ni concentration. The optical contrast in both the visible and near-infrared region increases with increasing Ni doping. At a light wavelength of 600 nm, the optical contrast enhanced from 50.9 to 86.0% at 0 and 1.5% Ni concentrations, respectively. Similarly, the CE is also higher at  $60.5 \text{ cm}^2 \text{ C}^{-1}$  for 1.5% Ni content compared with  $20.8 \text{ cm}^2 \text{ C}^{-1}$  for the undoped  $\text{WO}_3$  film. Notably, other doping techniques with different elements, such as Nb [154], Mo [155], Fe [156], and Ti [157], were shown to greatly improve the electrochromic performance of  $\text{WO}_3$  films. The most efficient strategy to develop the high-performance electrochromic  $\text{WO}_3$  films is the doping method [158], which requires further investigation from the community. To distinguish the electrochromic properties of different nanostructured  $\text{WO}_3$ , Table 1 summarizes and compares the key electrochromic metrics.

## 4.2 Molybdenum oxides

Similar to tungsten oxides, molybdenum oxides (e.g., molybdenum oxide, hydrated molybdenum oxide, and doped molybdenum oxide) are transparent in their oxidized state and become colored gray-blue on reduction. The layered crystalline structure of  $\text{MoO}_3$  allows it to exist in a quasi-two-dimensional state [159]. The ion intercalation capabilities, bandgap tunability, and various oxidation states allow  $\text{MoO}_3$  to be a promising electrochromic material [160]. Naturally,  $\text{MoO}_3$  exists in three phases: orthorhombic  $\alpha\text{-MoO}_3$ , monoclinic  $\beta\text{-MoO}_3$ , and hexagonal  $h\text{-MoO}_3$  [161]. The orthorhombic  $\alpha\text{-MoO}_3$  is the most stable phase of  $\text{MoO}_3$ . This phase is constituted by  $\text{MoO}_6$  octahedra that share edges and corners. The structure's unique layers parallel to the (010) plane provide open channels for guest ion intercalation (Figure 9A and B). However, molybdenum oxides suffer inferior cycling stability due to the large-volume expansion during the intercalation/deintercalation processes. As such, nanostructured molybdenum oxides in the form of nanoparticles [25], nanobelts [161], and nanosheets [162] have been shown to have improved electrochromic and electrochemical performances. Xie et al. reported on the fabrication of metastable hexagonal

**Table 1:** Summary of the electrochromic properties of nanostructured  $\text{WO}_3$  with different morphologies.

Ref.	Nanostructures	Optical contrast ( $\Delta T$ )	Switching time (s)	Coloration efficiency ( $\text{cm}^2 \text{ C}^{-1}$ )	Cycling numbers
Yao et al. [152]	$\text{WO}_3$ Quantum dots	97.8% at 633 nm	Coloration: 4.5 Bleaching: 4	76.8	20,000
Cong et al. [151]	$\text{WO}_3$ Quantum dots	94% at 633 nm	Coloration: 0.9 Bleaching: 1.0	154	50
Zhang et al. [146]	$\text{WO}_{3-x}$ nanocrystals	76% at 633 nm	Coloration: 4.5 Bleaching: 3.7	97.7	1000
Zhang et al. [47]	m- $\text{WO}_{3-x}$ nanowires	93.2% at 633 nm	Coloration: 16 Bleaching: 13	121	2000
Azam et al. [148]	$\text{WO}_3$ nanosheets	62.6% at 700 nm	Coloration: 10.7 Bleaching: 6.9	–	1000
Adhikari et al. [149]	$\text{WO}_3$ Nanofibers	43% at 550 nm	Coloration: 6.5 Bleaching: 4.0	63.15	500
Li et al. [150]	$\text{WO}_3$ Nanotrees	74.7% at 630 nm	Coloration: 7.3 Bleaching: 2.6	75.35	250
Li et al. [153]	$\text{WO}_3 \cdot 0.33\text{H}_2\text{O}$ Nanonests	57.6% at 633 nm	Coloration: 26 Bleaching: 5.5	126.34	1000
Zhou et al. [56]	Ni-doped $\text{WO}_3$ Nanorods	86% at 600 nm	Coloration: 19 Bleaching: 6.2	60.5	5500
Zhan et al. [157]	Ti-doped $\text{WO}_3$ Nanoplates	67.6% at 633 nm	Coloration: ~15 Bleaching: ~5	106.6	3000
Li et al. [126]	$\text{W}_{0.71}\text{Mo}_{0.29}\text{O}_{3-x}$ nanoparticles	42.9% at 633 nm	Coloration: 10 Bleaching: 7.5	36.3	2000
Li et al. [3]	Mo/Ti: $\text{WO}_3$ nanowires	76% at 633 nm	Coloration: 14 Bleaching: ~10	–	100



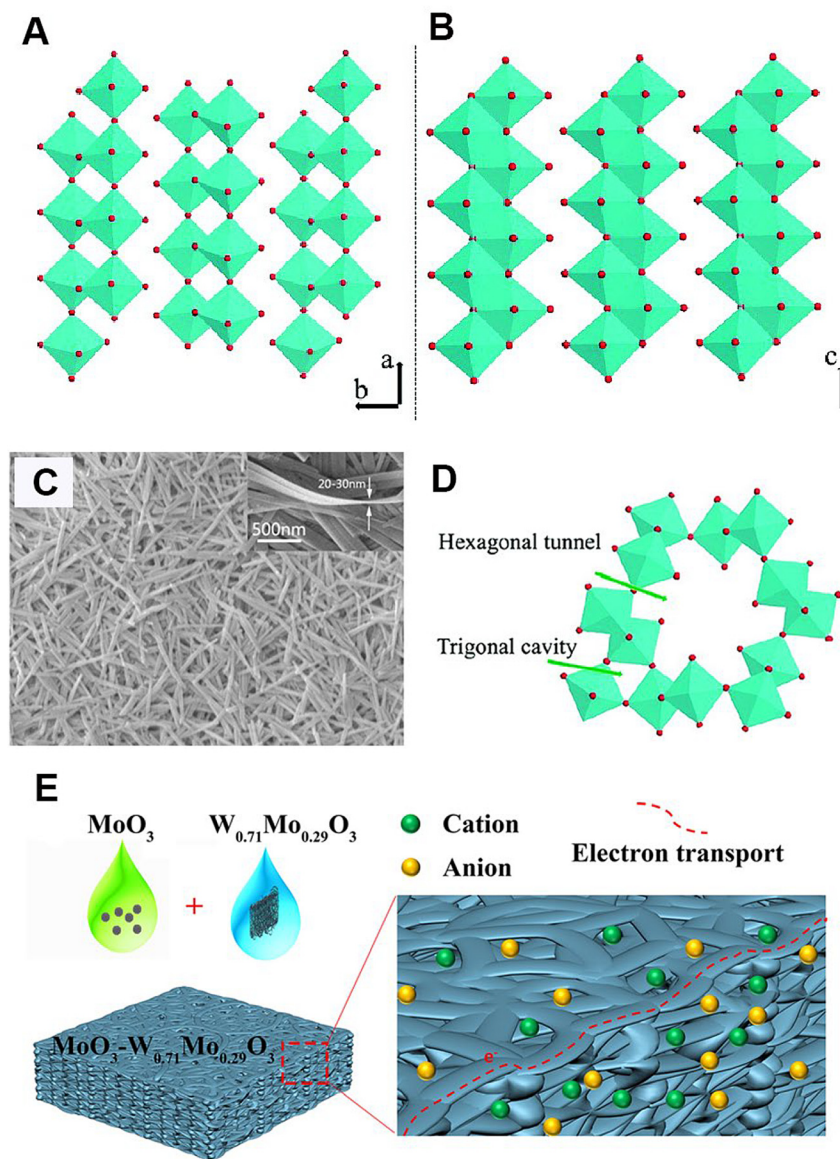


**Figure 9:** Structure and characterization of  $\text{MoO}_3$ -based electrochromic films.

(A–B) Schematic representation of orthorhombic  $\alpha$ - $\text{MoO}_3$ . (C) SEM image (inset is a cross-section view) of hexagonal  $\text{MoO}_3$  nanobelts. (D) Schematic representation of possible intercalation sites in hexagonal  $\text{MoO}_3$ . (A–D) Reproduced with permission from Ref. [161]. Copyright 2009, American Chemical Society. (E) Schematic illustration of the matrix effect of the  $\text{W}_{0.71}\text{Mo}_{0.29}\text{O}_3$  nanowires. Reproduced with permission from Ref. [25]. Copyright 2018, Elsevier.

$\text{MoO}_3$  nanobelts for electrochromic device applications (Figure 9C) [161]. The open channel structure of the hexagonal  $\text{MoO}_3$  nanobelts favors the efficient insertion of the guest ions (Figure 9D). As such, the  $\text{MoO}_3$  nanobelt films exhibit a more stable cycling performance than orthorhombic  $\alpha$ - $\text{MoO}_3$  films. Moreover, the nanohybridization of molybdenum oxide nanoparticles with tungsten molybdenum oxide nanowires offers an interesting electrochromic material platform as it circumvents many of the issues inherent to  $\text{MoO}_3$  (e.g., slow ionic transportation efficiency and volume expansion during cycling) [25]. Through a solution-processed method,  $\text{MoO}_3$  nanocrystals were embedded in the nanopores of  $\text{W}_{0.71}\text{Mo}_{0.29}\text{O}_3$  nanowire film to form a  $\text{MoO}_3$ - $\text{W}_{0.71}\text{Mo}_{0.29}\text{O}_3$  nanocomposite film (Figure 9E). The  $\text{W}_{0.71}\text{Mo}_{0.29}\text{O}_3$  nanowires not only serve as a buffer matrix which eliminates the large-volume expansion of

$\text{MoO}_3$  during the intercalation/deintercalation of guest ions, but also provides numerous charge transport pathways to enhance transport kinetics. Notably, the  $\text{MoO}_3$ - $\text{W}_{0.71}\text{Mo}_{0.29}\text{O}_3$  nanohybrid films show improved cycling stability compared with the intrinsic  $\text{MoO}_3$  films.

### 4.3 Titanium oxides

Titanium oxides (e.g., titanium oxide, hydrated titanium oxide, and doped titanium oxide) have been recognized as one of the most promising electrode materials for semiconductor electrochemistry [163]. Naturally, bulk titanium oxide exists in three crystalline phases: rutile, anatase, and brookite [164]. Refer to the crystal structure of titanium oxide,

the  $\text{Ti}^{4+}$  ions are surrounded by six  $\text{O}^{2-}$  ions creating an  $[\text{TiO}_6]$  octahedron, forming large vacant sites to accommodate guest ions. With the intercalation of guest ions, the transmittance of titanium oxide changes from a transparent state to a blue color. However, the electrochromic performance of intrinsic  $\text{TiO}_2$  is different from other open structures like  $\text{WO}_3$ . A recent report by Tong et al. demonstrated that a  $\text{TiO}_2$  mesoporous nanotube film exhibited an optical contrast of 33.5% at 700 nm, which is higher than the bulk  $\text{TiO}_2$  films due to the enhanced Li-ion insertion kinetics [165]. Although the optical contrast is enhanced via designing nanotube structures, the electrochromic effect is still lower than other electrochromic materials. This is attributed to the intrinsic moderate electrochromic effect of pure  $\text{TiO}_2$  [166]. As such, the aliovalent doping strategy is supposed the most convenient method to attain superior electrochromic effect of  $\text{TiO}_2$ -based electrochromic materials [167]. Hence, the focus of titanium oxide research has been shifted toward the synthesis of nanostructured doped- $\text{TiO}_2$  films. Recently, Cao and et al. synthesized Ta-doped  $\text{TiO}_2$  nanocrystals [168] (Figure 10A and B). The fabricated Ta-doped  $\text{TiO}_2$  thin films showed excellent electrochromic performance in terms of high optical contrast for both the visible and the near-infrared light spectra regions (i.e., 86.3% at 550 nm and 81.4% at 1600 nm). After 2000 cycles, the optical contrasts of Ta-doped  $\text{TiO}_2$  thin films

slightly decreased by 1.3 and 6.7% at 550 and 1600 nm, respectively, indicating good electrochemical stability. This Ta-doped  $\text{TiO}_2$  nanocrystal represents a promising new electrode material for smart windows applications [169].

Another dopant of  $\text{TiO}_2$  reported by Barawi et al. [36] to enhance the electrochromic performance of  $\text{TiO}_2$  is Nb. Four batches of Nb-doped  $\text{TiO}_2$  nanocrystals having different doping levels (from 0 to 15% of niobium content) were used to prepare highly transparent mesoporous electrodes. As shown in Figure 10C, the 10% Nb-doped  $\text{TiO}_2$  nanocrystals electrode exhibit the best electrochromic performance in both the visible and near-infrared light spectral regions. A dual-band (i.e., capable of independent control of visible light and near-infrared transmittance) electrochromic device was constructed using a 10% Nb-doped  $\text{TiO}_2$  nanocrystals electrode. This dual-band electrochromic device is capable of independent control of visible light and near-infrared transmittance, showing a 67% optical contrast at 2000 nm (Figure 10D).

#### 4.4 Vanadium oxides

By virtue of their multicolor behaviors, vanadium oxides are regarded as the most favorable inorganic materials for

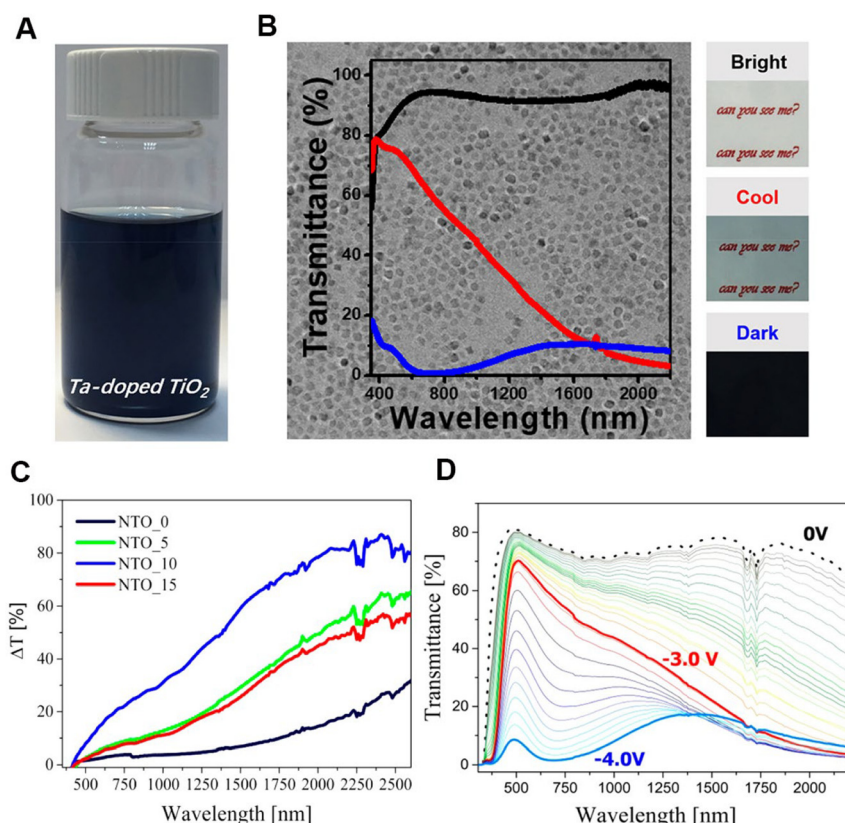


**Figure 10:** Structure and characterization of  $\text{TiO}_2$ -based electrochromic films. (A) Photograph of Ta-doped  $\text{TiO}_2$  nanocrystals dispersion in tetrachloroethylene. (B) Transmittance and corresponding photographs of Ta-doped  $\text{TiO}_2$  thin films electrode at different states. (A–B) Reproduced with permission from Ref. [168]. Copyright 2018, American Chemical Society. (C) Spectral variation of the optical transmittance at  $-1.6$  V for four batches of Nb-doped  $\text{TiO}_2$  nanocrystal films with different doping levels (from 0 to 15% of niobium content). (D) Transmittance spectra of a device embodying 10% Nb-doped  $\text{TiO}_2$  nanocrystals electrode at different bias potentials. Reproduced with permission from Ref. [36]. Copyright 2017, American Chemical Society.

electrochromic displays [125, 170, 171]. Vanadium cation exists in  $V^{2+}$ ,  $V^{3+}$ ,  $V^{4+}$ , and  $V^{5+}$  states in vanadium compounds, thus inducing the associated multicolor characteristics. While  $VO_2$  is known to be a thermochromic material [172],  $V_2O_3$  [173],  $V_3O_7$  [174], and  $V_2O_5$  [175] are found to have attractive electrochromic properties. The most widely investigated vanadium oxide is  $V_2O_5$ . With the intercalation/deintercalation of guest ions, this oxide offers reversible three-color states (i.e., yellow  $\rightleftharpoons$  green  $\rightleftharpoons$  blue) [23]. However, owing to their low electrical conductivity, significant volume expansion during cycling, and the slow reaction kinetics of bulk, intrinsic unstructured vanadium oxides have not been widely used in electrochromic devices [24]. In recent years, nanostructured vanadium oxides have been studied to mediate these drawbacks because the nanostructures shorten the diffusion paths of ions and provide abundant active sites on the surface. Steiner et al. demonstrated a self-supporting double-gyroid (DG) structure of  $V_2O_5$  (Figure 11A) [171]. The DG nanostructured  $V_2O_5$  possessed a highly ordered structure having 11 nm wide struts and a high specific surface-to-bulk volume ratio of  $161.4 \mu\text{m}^{-1}$ , leading to a fast and efficient lithium-ion intercalation/extraction process. The assembled electrochromic supercapacitor based on two opposite DG nanostructured  $V_2O_5$  electrodes is shown in Figure 11B, and its three-color displays (i.e., yellow, green, and blue) are presented in Figure 11C.

Extending the color palette for electrochromic devices is one of the major technological challenges in the field [5]. In 2020, Zhang et al. reported a transparent multicolor display enabled by Zn-based electrochromic devices [16]. The authors developed a method for synthesizing  $\text{NaV}_3\text{O}_8 \cdot 1.5\text{H}_2\text{O}$  (SVO) nanorods as an electrochromic material. The hydrated sodium ions, inserted between the  $V_3O_8$  layers, act as pillars to stabilize the layered structure (Figure 11D). The SVO film exhibits a reversible multicolor switch (orange  $\rightleftharpoons$  yellow  $\rightleftharpoons$  green) during  $\text{Zn}^{2+}$  insertion and extraction. The presence of sodium in SVO induces the orange color. A Zn-SVO device was assembled via sandwiching a Zn frame anode and a gel electrolyte (polyvinyl alcohol– $\text{ZnSO}_4$ ) between two SVO electrodes (Figure 11E). Through the combination of two SVO electrode segments, the color overlay effect broadened the resultant color palettes of the Zn-SVO display. Figure 11F illustrates the color overlay effect obtained by superimposing the orange, yellow, and green colors. Because the two SVO electrode segments can be colored and bleached independently, the Zn-SVO device can display six colors (i.e., orange, amber, yellow, brown, chartreuse, and green) (Figure 11G).

## 4.5 Nickel oxides

As typical anodic electrochromic materials, serving as complementary material to tungsten oxides when assembling a device, nickel oxides (e.g., nickel oxide, hydrated nickel oxide, and doped nickel oxide) are known for their high coloration efficiency and optical contrast [59]. In contrast to the cathodic electrochromic materials such as  $\text{WO}_3$ , the colored state of NiO is caused by electrochemical oxidation, with anion insertion ( $\text{OH}^-$ ) or cation extraction ( $\text{Li}^+$ ) [58]. On the other hand, the NiO films become bleached by electrochemical reduction. The NiO film exhibits a reversible color change that switches between brown color and transparent state [176]. Similar to other intrinsic oxide electrochromic materials, critical issues, such as slow switching speed, low color contrast, and poor cycle durability of NiO limit its practical utility in electrochromic devices [177, 178]. Enhanced electrochromic performances of NiO thin films have been recently achieved through nanostructured NiO films. Boo et al. reported a nanoporous NiO thin film fabricated by chemical bath deposition [55]. The nanoporous NiO thin films having high porosity showed excellent electrochromic properties, with a transmittance change of 77% at 550 nm and a coloration efficiency of  $99.5 \text{ cm}^2 \text{ C}^{-1}$ . Liou et al. described the growth of NiO nanorods via hot-filament metal-oxide vapor deposition where large-area arrays of one-dimensional NiO nanorods were grown on a conducting ITO film [179]. The NiO nanorod films showed excellent electrochromic performance, including high optical transmittance difference (60%), large diffusion coefficient ( $\sim 6.33 \times 10^{-8} \text{ cm}^2 \text{ s}^{-1}$ ), and very fast coloration and bleaching times (1.55 and 1.22 s).

An interesting platform of nanostructured NiO thin films is the one prepared by inkjet printing of NiO nanoparticles [181]. Inkjet printing is a low-cost and efficient technology for patterning and deposition of multilayered nanostructured materials on various substrates. The printed NiO film, with nine printed layers, exhibited an optical contrast of 64.2% at 550 nm and a coloration efficiency of  $136.7 \text{ cm}^2 \text{ C}^{-1}$ . Moreover, by doping NiO with other elements, such as Cu [182], Al [176], and Co [180], the material electrochromic performance was greatly enhanced. As shown in Figure 12A–F, with an increase in Co doping (from 0 to 3%), the thickness of the formed NiO film becomes thin and the pore diameter of the nanoflakes decreases [180]. However, nanoflake-shaped NiO films cannot form when the amount of Co doping reaches 3%. This suggests that an optimum Co doping concentration is required for electrochromic applications. In this regard, the 1% Co-doped NiO nanoflake array film exhibited an outstanding optical



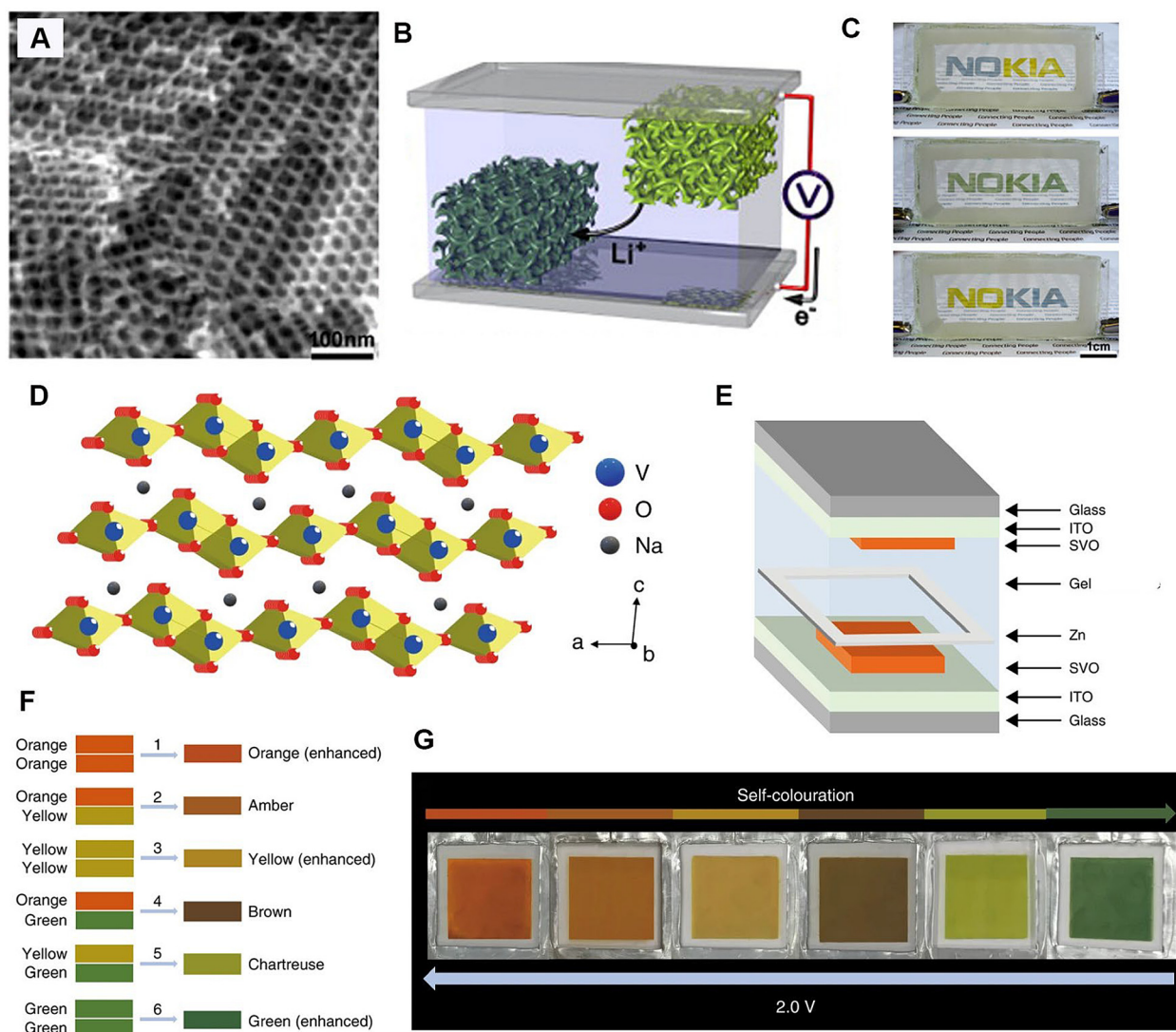


**Figure 11:** Structure and characterization of vanadium oxide-based electrochromic displays.

(A) Scanning electron microscope (SEM) of a mesoporous  $V_2O_5$  double-gyroid film on an FTO substrate (B) Schematic illustration of the electrochromic supercapacitor design based on two laterally offset double-gyroid structured electrodes. (C) Photographs of an electrochromic supercapacitor device displaying color change on charge and discharge. The letters "NO" form the double-gyroid structured top electrode and "KIA" form the bottom electrode. (A–C) Reproduced with permission from Ref. [171]. Copyright 2012, American Chemical Society. (D) Crystal structure of the SVO nanorods. (E) Schematic illustration of the Zn-SVO electrochromic display. (F) Schematic illustration of the color overlay effect via the combination of orange, yellow, and green colors. (G) Digital photographs of the Zn-SVO display showing six colors obtained through the color overlay effect. Reproduced with permission from Ref. [16]. Copyright 2020, Nature Publishing Group.

contrast of 88.3% at 550 nm. Most recently, Liang et al. developed a self-templating method to build up metal-organic framework-derived hierarchical-porous carbon-embedded nickel oxide nanoparticle ( $NiO@C$ ) films for high-performance electrochromism [62]. Figure 12G illustrates the preparation procedures of the hierarchical-porous  $NiO@C$  electrodes. As a result, the hierarchical-porous  $NiO@C$  electrodes with both good ion diffusion and electrical conductivity were achieved. This electrode showed a fast switching speed (0.46/0.25 s for coloring/

bleaching), high coloration efficiency ( $113.5 \text{ cm}^2 \text{ C}^{-1}$ ), and excellent cycling stability (90.1% after 20,000 cycles).

## 4.6 Cobalt oxides

Cobalt oxide normally exists in three different polymorphs:  $CoO$ ,  $Co_3O_4$ , and  $Co_2O_3$  [183]. Among them, the crystalline  $Co_3O_4$  phase has been widely studied because of its thermodynamic stability and electrochemical properties [184].

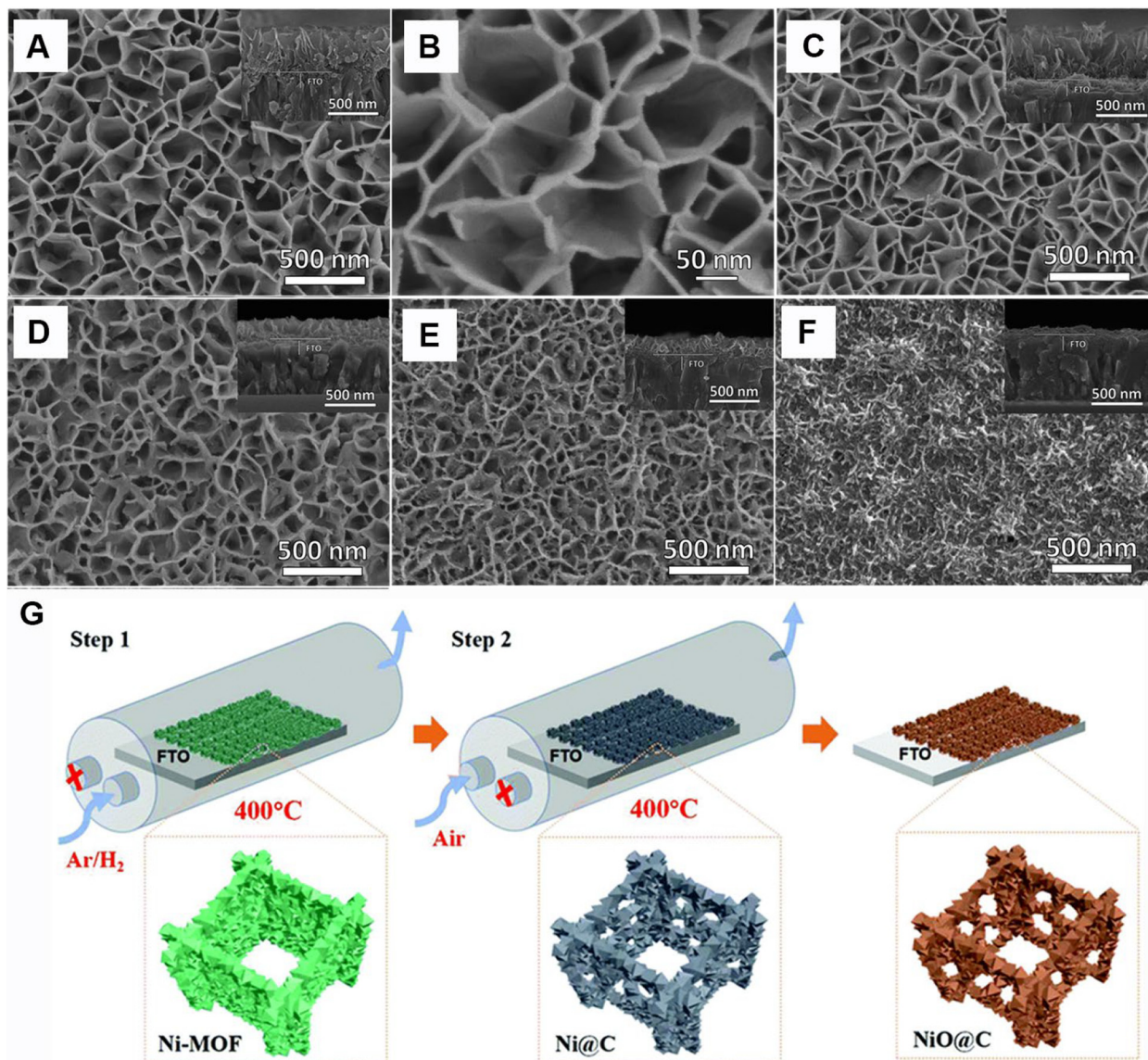


**Figure 12:** Characterization of NiO-based electrochromic films.

Scanning electron microscope (SEM) images of the films: (A and B) undoped NiO, (C) NiO–Co 0.3%, (D) NiO–Co 0.5%, (E) NiO–Co 1%, and (F) NiO–Co 3% (cross-sectional view is presented in the inset). Reproduced with permission from Ref. [180]. Copyright 2014, Royal Society of Chemistry. (G) Preparation procedures of the hierarchical-porous NiO@C electrode. Reproduced with permission from Ref. [62]. Copyright 2019, Royal Society of Chemistry.

Co<sub>3</sub>O<sub>4</sub> exhibits a reversible color change between a yellow-brown and dark brown under potential cycling [185]. Similar to other metal oxides suffering the large-volume expansion during the coloration and bleaching processes, Co<sub>3</sub>O<sub>4</sub> suffers from structural decomposition, poor stability, and cation kinetics. To minimize such shortcomings, several reports described the growth of nanostructured Co<sub>3</sub>O<sub>4</sub> thin films for electrochromic applications. Xia et al. demonstrated a facile method for synthesizing ordered bowl-like Co<sub>3</sub>O<sub>4</sub> arrays [186]. The as-prepared Co<sub>3</sub>O<sub>4</sub> films had a hierarchical porous structure (Figure 13A) when

annealed at 200 °C, and it exhibits reversible color switchings between dark gray and pale yellow (Figure 13B). The coloration efficiency was calculated to be 29 cm<sup>2</sup> C<sup>−1</sup> at 633 nm, with an optical contrast of up to 33%. Notably, owing to the microporous structures, the bowl-like Co<sub>3</sub>O<sub>4</sub> arrays are found to have good electrochemical stability.

The aforementioned strategies for developing nanostructured inorganic electrochromic materials are mainly focused on the solution process techniques. This nanofabrication process has several advantages, such as low-cost, ease of designing nanostructures, and fast switching



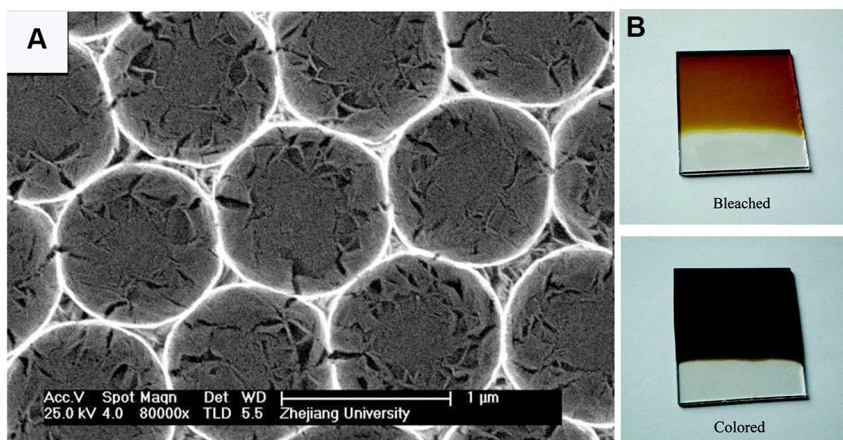


**Figure 13:** Characterization of Co<sub>3</sub>O<sub>4</sub>-based electrochromic films.

(A) Scanning electron microscope (SEM) images of the Co<sub>3</sub>O<sub>4</sub> film annealed at 200 °C for 1 h. (B) Photographs of the Co<sub>3</sub>O<sub>4</sub> electrode with a size of 1.5 × 1.5 cm<sup>2</sup> in the colored and bleached states. Reproduced with permission from Ref. [186]. Copyright 2010, American Chemical Society.

times which allow the fabrication of electrochromic material having kinetics compared to the vacuum deposition methods. To further enhance their electrochemical stability, future research needs to be focused on the interface engineering of the solution-processed nanostructured films, via strengthening the adhesion between the nanostructural electrochromic layers and the substrates. Notwithstanding, there is still a need for innovative designs of high-performance nanostructural inorganic electrochromic films to make the electrochromic device more practical for light control applications.

## 5 Outlook and future challenges

This review summarizes the recent progress of nanostructured inorganic electrochromic materials, which we hope to be helpful to those scientists who have recently entered this field. The classification of common electrochromic materials is outlined as inorganic, organic, inorganic–organic hybrids, and plasmonic materials. The evaluation metrics for electrochromic materials, including color and optical contrast, coloration efficiency, switching time, and cycling stability are discussed. Electrochromic properties and synthetic methods for different nanostructured electrochromic materials are evaluated based on structure/morphology engineering, doping techniques, and crystal phase designs. Although the field of nanostructured inorganic electrochromic materials has witnessed rapid development and remarkable achievements, there are still some major challenges that hinder the high performance of electrochromic materials and their real-world applications: 1. Most of the electrochromic performance tests were conducted based on a single electrode but not a device. However, there are enormous differences between a single electrode and a device in terms of electrochromic performance. Because a device is required for

practical use, future research of electrochromism should be more focused on the assembly of an electrochromic device, especially large area devices as the size exerts a significant effect on both the switching times and color uniformity. 2. The practical use of electrochromic materials requires long-term durability favoring innovative designs of robust nanostructured inorganic electrochromic layers. As such, a better understanding of the interface engineering between the electrochromic layers and the substrates is critical to promote performance and to enhance stability. 3. The multifunctional electrochromic devices (e.g., electrochromic supercapacitors [5, 85], electrochromic batteries [2, 3], and electrochromic fibers [187, 188]) are poised for future development of novel electrochromic devices. Exploring nanostructured material functionalities will provide additional avenues for multifunctional electrochromic devices.

Such key issues illustrate the importance of understanding electrochromic materials on the nanoscale and processing compatibility of electrochromic devices on a large scale. With the recent achievement regarding the designs of nanostructured inorganic electrochromic materials, future efforts should demonstrate the electrochromic devices to meet real-world applications, such as durable smart windows, multicolor inorganic displays, and color-tunable optical devices.

**Acknowledgments:** This work was supported by the Natural Sciences and Engineering Research Council of Canada (Grant File No: CRDPJ 509210-17), Alberta Innovates, and All Weather Windows Ltd.

**Author contribution:** All the authors have accepted responsibility for the entire content of this submitted manuscript and approved submission.

**Research funding:** This work was supported by the Natural Sciences and Engineering Research Council of Canada (Grant File No: CRDPJ 509210-17), Alberta Innovates, and All Weather Windows Ltd.



**Conflict of interest statement:** The authors declare no conflicts of interest regarding this article.

## References

- [1] B. A. Korgel, "Composite for smarter windows," *Nature*, vol. 500, pp. 278–279, 2013.
- [2] H. Z. Li, C. J. Firby, and A. Y. Elezzabi, "Rechargeable aqueous hybrid  $\text{Zn}^{2+}/\text{Al}^{3+}$  electrochromic batteries," *Joule*, vol. 3, pp. 2268–2278, 2019.
- [3] H. Z. Li, L. McRae, C. J. Firby, and A. Y. Elezzabi, "Rechargeable aqueous electrochromic batteries utilizing Ti-substituted tungsten molybdenum oxide based  $\text{Zn}^{2+}$  ion intercalation cathodes," *Adv. Mater.*, vol. 31, p. 1807065, 2019.
- [4] S. L. Zhang, S. Cao, T. R. Zhang, et al., "Overcoming the technical challenges in Al anode-based electrochromic energy storage windows," *Small Methods*, vol. 4, p. 1900545, 2020.
- [5] J. Chen, Z. Wang, Z. G. Chen, S. Cong, and Z. G. Zhao, "Fabry-Perot cavity-type electrochromic supercapacitors with exceptionally versatile color tunability," *Nano Lett.*, vol. 20, pp. 1915–1922, 2020.
- [6] C. J. Barile, D. J. Slotcavage, J. Y. Hou, M. T. Strand, T. S. Hernandez, and M. D. McGehee, "Dynamic windows with neutral color, high contrast, and excellent durability using reversible metal electrodeposition," *Joule*, vol. 1, pp. 133–145, 2017.
- [7] D. D. Miller, J. Y. Li, S. M. Islam, J. F. Jeanetta, and C. J. Barile, "Aqueous alkaline electrolytes for dynamic windows based on reversible metal electrodeposition with improved durability," *J. Mater. Chem. C*, vol. 8, pp. 1826–1834, 2020.
- [8] S. Zhang, S. Cao, T. Zhang, and J. Y. Lee, "Plasmonic Oxygen-deficient  $\text{TiO}_{2-x}$  nanocrystals for dual-band electrochromic smart windows with efficient energy recycling," *Adv. Mater.*, p. 2004686, 2020, <https://doi.org/10.1002/adma.202004686>.
- [9] K. Bange and T. Gambke, "Electrochromic materials for optical switching devices," *Adv. Mater.*, vol. 2, pp. 10–16, 1990.
- [10] Y. Y. Wang, S. Wang, X. J. Wang, et al., "A multicolour bistable electronic shelf label based on intramolecular proton-coupled electron transfer," *Nat. Mater.*, vol. 18, pp. 1335–1342, 2019.
- [11] C. M. Amb, A. L. Dyer, and J. R. Reynolds, "Navigating the color palette of solution-processable electrochromic polymers," *Chem. Mater.*, vol. 23, pp. 397–415, 2011.
- [12] P. J. Shi, C. M. Amb, E. P. Knott, et al., "Broadly absorbing black to transmissive switching electrochromic polymers," *Adv. Mater.*, vol. 22, pp. 4949–4953, 2010.
- [13] X. Wang, K. Chen, L. S. de Vasconcelos, et al., "Mechanical breathing in organic electrochromics," *Nat. Commun.*, vol. 11, p. 211, 2020.
- [14] S. Xiong, Y. Wang, X. Wang, et al., "Schiff base type conjugated organic framework nanofibers: solvothermal synthesis and electrochromic properties," *Sol. Energy Mater. Sol. Cells*, vol. 209, p. 110438, 2020.
- [15] F. S. Han, M. Higuchi, and D. G. Kurth, "Metallo-supramolecular polymers based on functionalized bis-terpyridines as novel electrochromic materials," *Adv. Mater.*, vol. 19, pp. 3928–3931, 2007.
- [16] W. Zhang, H. Li, W. W. Yu, and A. Y. Elezzabi, "Transparent inorganic multicolour displays enabled by zinc-based electrochromic devices," *Light Sci. Appl.*, vol. 9, p. 121, 2020.
- [17] Z. Wang, X. Y. Wang, S. Cong, et al., "Towards full-colour tunability of inorganic electrochromic devices using ultracompact fabry-perot nanocavities," *Nat. Commun.*, vol. 11, p. 302, 2020.
- [18] H. Eric, H. Z. Li, and A. Y. Elezzabi, "Rechargeable  $\text{Zn}^{2+}/\text{Al}^{3+}$  dual-ion electrochromic device with long life time utilizing dimethyl sulfoxide (DMSO)-nanocluster modified hydrogel electrolytes," *RSC Adv.*, vol. 9, pp. 32047–32057, 2019.
- [19] L. L. Xie, S. W. Zhao, Y. Zhu, et al., "High performance and excellent stability of all-solid-state electrochromic devices based on a  $\text{Li}_{1.85}\text{AlO}_2$  ion conducting layer," *ACS Sustain. Chem. Eng.*, vol. 7, pp. 17390–17396, 2019.
- [20] H. Yu, J. J. Guo, C. Wang, et al., "High performance in electrochromic amorphous  $\text{WO}_x$  film with long-term stability and tunable switching times via Al/Li-ions intercalation/deintercalation," *Electrochim. Acta*, vol. 318, pp. 644–650, 2019.
- [21] S. L. Zhang, Y. Li, T. R. Zhang, et al., "Dual-band electrochromic devices with a transparent conductive capacitive charge-balancing anode," *ACS Appl. Mater. Interfaces*, vol. 11, pp. 48062–48070, 2019.
- [22] W. Zhang, H. Z. Li, C. J. Firby, M. Al-Hussein, and A. Y. Elezzabi, "Oxygen-vacancy-tunable electrochemical properties of electrodeposited molybdenum oxide films," *ACS Appl. Mater. Interfaces*, vol. 11, pp. 20378–20385, 2019.
- [23] Z. Q. Tong, N. Li, H. M. Lv, et al., "Annealing synthesis of coralline  $\text{V}_2\text{O}_5$  nanorod architecture for multicolor energy-efficient electrochromic device," *Sol. Energy Mater. Sol. Cells*, vol. 146, pp. 135–143, 2016.
- [24] K. Zhang, N. Li, X. X. Ma, et al., "Building ultrathin polyaniline encapsulated  $\text{V}_2\text{O}_5$  heterogeneous nanowires and its electrochromic performance," *J. Electroanal. Chem.*, vol. 825, pp. 16–21, 2018.
- [25] H. Z. Li, L. McRae, C. J. Firby, M. Al-Hussein, and A. Y. Elezzabi, "Nanohybridization of molybdenum oxide with tungsten molybdenum oxide nanowires for solution-processed fully reversible switching of energy storing smart windows," *Nano Energy*, vol. 47, pp. 130–139, 2018.
- [26] G. F. Cai, P. Darmawan, X. Cheng, and P. S. Lee, "Inkjet printed large area multifunctional smart windows," *Adv. Energy Mater.*, vol. 7, p. 1602598, 2017.
- [27] D. Y. Ma and J. M. Wang, "Inorganic electrochromic materials based on tungsten oxide and nickel oxide nanostructures," *Sci. China Chem.*, vol. 60, pp. 54–62, 2017.
- [28] Y. Y. Song, Z. D. Gao, J. H. Wang, X. H. Xia, and R. Lynch, "Multistage coloring electrochromic device based on  $\text{TiO}_2$  nanotube arrays modified with  $\text{WO}_3$  nanoparticles," *Adv. Funct. Mater.*, vol. 21, pp. 1941–1946, 2011.
- [29] G. F. Cai, J. X. Wang, and P. S. Lee, "Next-generation multifunctional electrochromic devices," *Acc. Chem. Res.*, vol. 49, pp. 1469–1476, 2016.
- [30] Z. Wang, X. Y. Wang, S. Cong, F. X. Geng, and Z. G. Zhao, "Fusing electrochromic technology with other advanced technologies: a new roadmap for future development," *Mater. Sci. Eng. R*, vol. 140, p. 100524, 2020.
- [31] Y. Ke, J. Chen, G. Lin, et al., "Smart windows: electro-, thermo-, mechano-, photochromics, and beyond," *Adv. Energy Mater.*, vol. 9, p. 1902066, 2019.
- [32] J. Kim, M. Rémond, D. Kim, H. Jang, and E. Kim, "Electrochromic conjugated polymers for multifunctional smart windows with integrative functionalities," *Adv. Mater. Technol.*, vol. 5, p. 1900890, 2020.

- [33] P. H. Yang, P. Sun, and W. J. Mai, "Electrochromic energy storage devices," *Mater. Today*, vol. 19, pp. 394–402, 2016.
- [34] K. J. Patel, G. G. Bhatt, J. R. Ray, P. Suryavanshi, and C. J. Panchal, "All-inorganic solid-state electrochromic devices: a review," *J. Solid State Electrochem.*, vol. 21, pp. 337–347, 2017.
- [35] P. Jittiarporn, S. Badilescu, M. N. Al Sawaf, L. Sikong, and V. V. Truong, "Electrochromic properties of sol-gel prepared hybrid transition metal oxides – a short review," *J. Sci. Adv. Mater. Devices*, vol. 2, pp. 286–300, 2017.
- [36] M. Barawi, L. De Trizio, R. Giannuzzi, G. Veramonti, L. Manna, and M. Manca, "Dual band electrochromic devices based on Nb-doped TiO<sub>2</sub> nanocrystalline electrodes," *ACS Nano*, vol. 11, pp. 3576–3584, 2017.
- [37] X. Q. Che, Z. H. Wu, G. B. Dong, et al., "Properties of all-thin-film glass/ITO/WO<sub>3</sub>:H/Ta<sub>2</sub>O<sub>5</sub>/NiO<sub>x</sub>/ITO electrochromic devices prepared by magnetron sputtering," *Thin Solid Films*, vol. 662, pp. 6–12, 2018.
- [38] W. J. Dong, Y. Lv, L. L. Xiao, Y. Fan, N. Zhang, and X. Y. Liu, "Bifunctional MoO<sub>3</sub>-WO<sub>3</sub>/Ag/MoO<sub>3</sub>-WO<sub>3</sub> Films for efficient ITO-free electrochromic devices," *ACS Appl. Mater. Interfaces*, vol. 8, pp. 33842–33847, 2016.
- [39] G. K. Ong, C. A. S. Cabezas, M. N. Dominguez, S. L. Skjaervo, S. Heo, and D. J. Milliron, "Electrochromic niobium oxide nanorods," *Chem. Mater.*, vol. 32, pp. 468–475, 2020.
- [40] X. Zhang, Y. L. Tian, W. J. Li, et al., "Preparation and performances of all-solid-state variable infrared emittance devices based on amorphous and crystalline WO<sub>3</sub> electrochromic thin films," *Sol. Energy Mater. Sol. Cells*, vol. 200, p. 109916, 2019.
- [41] Q. Zhao, Y. S. Fang, K. Qiao, W. Wei, Y. J. Yao, and Y. F. Gao, "Printing of WO<sub>3</sub>/ITO nanocomposite electrochromic smart windows," *Sol. Energy Mater. Sol. Cells*, vol. 194, pp. 95–102, 2019.
- [42] C. G. Granqvist, "Electrochromic materials: microstructure, electronic bands, and optical properties," *Appl. Phys. A*, vol. 57, pp. 3–12, 1993.
- [43] S. Cong, F. X. Geng, and Z. G. Zhao, "Tungsten oxide materials for optoelectronic applications," *Adv. Mater.*, vol. 28, pp. 10518–10528, 2016.
- [44] X. F. Li, K. Perera, J. Z. He, A. Gumyusenge, and J. G. Mei, "Solution-processable electrochromic materials and devices: roadblocks and strategies towards large-scale applications," *J. Mater. Chem. C*, vol. 7, pp. 12761–12789, 2019.
- [45] E. L. Runnerstrom, A. Llordes, S. D. Lounis, and D. J. Milliron, "Nanostructured electrochromic smart windows: traditional materials and NIR-selective plasmonic nanocrystals," *Chem. Commun.*, vol. 50, pp. 10555–10572, 2014.
- [46] C. G. Granqvist, "Electrochromics for smart windows: oxide-based thin films and devices," *Thin Solid Films*, vol. 564, pp. 1–38, 2014.
- [47] S. L. Zhang, S. Cao, T. R. Zhang, A. Fisher, and J. Y. Lee, "Al<sup>3+</sup> intercalation/de-intercalation-enabled dual-band electrochromic smart windows with a high optical modulation, quick response and long cycle life," *Energy Environ. Sci.*, vol. 11, pp. 2884–2892, 2018.
- [48] W. Zhang, H. Z. Li, M. Al-Hussein, and A. Y. Elezzabi, "Electrochromic battery displays with energy retrieval functions using solution-processable colloidal vanadium oxide nanoparticles," *Adv. Opt. Mater.*, vol. 8, p. 1901224, 2020.
- [49] S. Bulja, R. Kopf, K. Nolan, et al., "Tuneable dielectric and optical characteristics of tailor-made inorganic electrochromic materials," *Sci. Rep.*, vol. 7, p. 13484, 2017.
- [50] D. T. Gillaspie, R. C. Tenent, and A. C. Dillon, "Metal-oxide films for electrochromic applications: present technology and future directions," *J. Mater. Chem.*, vol. 20, pp. 9585–9592, 2010.
- [51] S. A. Majeed, B. Ghazal, D. E. Nevenon, et al., "Evaluation of the intramolecular charge-transfer properties in solvatochromic and electrochromic zinc octa(carbazolyl)phthalocyanines," *Inorg. Chem.*, vol. 56, pp. 11640–11653, 2017.
- [52] Y. S. Nam, H. Park, A. P. Magyar, D. S. Yun, T. S. Pollom, and A. M. Belcher, "Virus-templated iridium oxide-gold hybrid nanowires for electrochromic application," *Nanoscale*, vol. 4, pp. 3405–3409, 2012.
- [53] Y. Ren, X. G. Zhou, H. Zhang, L. Lei, and G. Y. Zhao, "Preparation of a porous NiO array-patterned film and its enhanced electrochromic performance," *J. Mater. Chem. C*, vol. 6, pp. 4952–4958, 2018.
- [54] N. Sakai, Y. Ebina, K. Takada, and T. Sasaki, "Electrochromic films composed of MnO<sub>2</sub> nanosheets with controlled optical density and high coloration efficiency," *J. Electrochem. Soc.*, vol. 152, pp. E384–E389, 2005.
- [55] H. Yang, J. H. Yu, H. J. Seo, R. H. Jeong, and J. H. Boo, "Improved electrochromic properties of nanoporous NiO film by NiO flake with thickness controlled by aluminum," *Appl. Surf. Sci.*, vol. 461, pp. 88–92, 2018.
- [56] J. Zhou, Y. Wei, G. Luo, J. Zheng, and C. Xu, "Electrochromic properties of vertically aligned Ni-doped WO<sub>3</sub> nanostructure films and their application in complementary electrochromic devices," *J. Mater. Chem. C*, vol. 4, pp. 1613–1622, 2016.
- [57] L. Liu, K. Du, Z. He, et al., "High-temperature adaptive and robust ultra-thin inorganic all-solid-state smart electrochromic energy storage devices," *Nano Energy*, vol. 62, pp. 46–54, 2019.
- [58] J. Guo, M. Wang, G. Dong, et al., "Mechanistic insights into the coloration, evolution, and degradation of NiO<sub>x</sub> electrochromic anodes," *Inorg. Chem.*, vol. 57, pp. 8874–8880, 2018.
- [59] Q. R. Liu, Q. Q. Chen, Q. Q. Zhang, et al., "In situ electrochromic efficiency of a nickel oxide thin film: origin of electrochemical process and electrochromic degradation," *J. Mater. Chem. C*, vol. 6, pp. 646–653, 2018.
- [60] D. Ma, G. Shi, H. Wang, Q. Zhang, and Y. Li, "Hierarchical NiO microflake films with high coloration efficiency, cyclic stability and low power consumption for applications in a complementary electrochromic device," *Nanoscale*, vol. 5, pp. 4808–4815, 2013.
- [61] I. Bouessaya, A. Rougier, P. Poizot, J. Moscovici, A. Michalowicz, and J. M. Tarascon, "Electrochromic degradation in nickel oxide thin film: a self-discharge and dissolution phenomenon," *Electrochim. Acta*, vol. 50, pp. 3737–3745, 2005.
- [62] H. Liang, R. Li, C. Li, et al., "Regulation of carbon content in MOF-derived hierarchical-porous NiO@C films for high-performance electrochromism," *Mater. Horiz.*, vol. 6, pp. 571–579, 2019.
- [63] W. Kang, C. Yan, X. Wang, et al., "Green synthesis of nanobelt-membrane hybrid structured vanadium oxide with high electrochromic contrast," *J. Mater. Chem. C*, vol. 2, pp. 4727–4732, 2014.
- [64] J. M. Wang, L. Zhang, L. Yu, et al., "A bi-functional device for self-powered electrochromic window and self-rechargeable transparent battery applications," *Nat. Commun.*, vol. 5, p. 4921, 2014.
- [65] Y. Yue, H. Li, K. Li, et al., "High-performance complementary electrochromic device based on WO<sub>3</sub>·0.33H<sub>2</sub>O/PEDOT and prussian blue electrodes," *J. Phys. Chem. Solids*, vol. 110, pp. 284–289, 2017.

- [66] J. H. Qian, D. Y. Ma, Z. P. Xu, D. Li, and J. M. Wang, "Electrochromic properties of hydrothermally grown Prussian blue film and device," *Sol. Energy Mater. Sol. Cells*, vol. 177, pp. 9–14, 2018.
- [67] Z. Wang, Q. Z. Zhang, S. Cong, et al., "Using intrinsic intracrystalline tunnels for near-infrared and visible-light selective electrochromic modulation," *Adv. Opt. Mater.*, vol. 5, p. 1700194, 2017.
- [68] B. Wang, M. W. Cui, Y. F. Gao, et al., "A long-life battery-type electrochromic window with remarkable energy storage ability," *Solar RRL*, vol. 4, p. 1900425, 2020.
- [69] H. Z. Li and A. Y. Elezzabi, "Simultaneously enabling dynamic transparency control and electrical energy storage via electrochromism," *Nanoscale Horiz.*, vol. 5, pp. 691–695, 2020.
- [70] H. Li, W. Zhang, and A. Y. Elezzabi, "Transparent zinc-mesh electrodes for solar-charging electrochromic windows," *Adv. Mater.*, p. 2003574, 2020, <https://doi.org/10.1002/adma.202003574>.
- [71] C. D. Wessells, R. A. Huggins, and Y. Cui, "Copper hexacyanoferrate battery electrodes with long cycle life and high power," *Nat. Commun.*, vol. 2, p. 550, 2011.
- [72] C. D. Wessells, S. V. Peddada, M. T. McDowell, R. A. Huggins, and Y. Cui, "The effect of insertion species on nanostructured open framework hexacyanoferrate battery electrodes," *J. Electrochem. Soc.*, vol. 159, pp. A98–A103, 2012.
- [73] B. Anasori, M. R. Lukatskaya, and Y. Gogotsi, "2D metal carbides and nitrides (MXenes) for energy storage," *Nat. Rev. Mater.*, vol. 2, p. 16098, 2017.
- [74] P. Salles, D. Pinto, K. Hantanasirisakul, K. Maleski, C. E. Shuck, and Y. Gogotsi, "Electrochromic effect in titanium carbide MXene thin films produced by dip-coating," *Adv. Funct. Mater.*, vol. 29, p. 1809223, 2019.
- [75] K. W. Shah, S. X. Wang, D. X. Y. Soo, and J. W. Xu, "Viologen-based electrochromic materials: from small molecules, polymers and composites to their applications," *Polymers*, vol. 11, p. 1839, 2019.
- [76] E. Dmitrieva, M. Rosenkranz, Y. Alesanco, and A. Vinuales, "The reduction mechanism of p-cyanophenylviologen in PVA-borax gel polyelectrolyte-based bicolor electrochromic devices," *Electrochim. Acta*, vol. 292, pp. 81–87, 2018.
- [77] B. Gelinas, D. Das, and D. Rochefort, "Air-stable, self-bleaching electrochromic device based on viologen-and ferrocene-containing triflimide redox ionic liquids," *ACS Appl. Mater. Interfaces*, vol. 9, pp. 28726–28736, 2017.
- [78] P. Camurlu, "Polypyrrole derivatives for electrochromic applications," *RSC Adv.*, vol. 4, pp. 55832–55845, 2014.
- [79] M. Ghoorchian, F. Tavoli, and N. Alizadeh, "Long-term stability of nanostructured polypyrrole electrochromic devices by using deep eutectic solvents," *J. Electroanal. Chem.*, vol. 807, pp. 70–75, 2017.
- [80] W. T. Neo, Q. Ye, S. J. Chua, and J. W. Xu, "Conjugated polymer-based electrochromics: materials, device fabrication and application prospects," *J. Mater. Chem. C*, vol. 4, pp. 7364–7376, 2016.
- [81] L. Gomes, A. Branco, T. Moreira, F. Feliciano, C. Pinheiro, and C. Costa, "Increasing the electrical conductivity of electrochromic PEDOT: PSS films – a comparative study," *Sol. Energy Mater. Sol. Cells*, vol. 144, pp. 631–640, 2016.
- [82] F. Hu, H. C. Peng, S. H. Zhang, Y. C. Gu, B. Yan, and S. Chen, "PEDOT nanoparticles fully covered on natural tubular clay for hierarchically porous electrochromic film," *Sol. Energy Mater. Sol. Cells*, vol. 199, pp. 59–65, 2019.
- [83] T. G. Yun, M. Park, D. H. Kim, et al., "All-transparent stretchable electrochromic supercapacitor wearable patch device," *ACS Nano*, vol. 13, pp. 3141–3150, 2019.
- [84] D. Levasseur, I. Mjejri, T. Rolland, and A. Rougier, "Color tuning by oxide addition in PEDOT: PSS-based electrochromic devices," *Polymers*, vol. 11, p. 179, 2019.
- [85] X. L. Chen, H. J. Lin, J. Deng, et al., "Electrochromic fiber-shaped supercapacitors," *Adv. Mater.*, vol. 26, pp. 8126–8132, 2014.
- [86] K. L. Zhou, H. Wang, J. T. Jiu, J. B. Liu, H. Yan, and K. Suganuma, "Polyaniline films with modified nanostructure for bifunctional flexible multicolor electrochromic and supercapacitor applications," *Chem. Eng. J.*, vol. 345, pp. 290–299, 2018.
- [87] Q. Lu, X. Zhang, W. Cai, et al., "Donor–acceptor conjugated polymers containing isoindigo block for novel multifunctional materials for electrochromic, resistance memory, and detector devices," *Sol. Energy Mater. Sol. Cells*, vol. 200, p. 109979, 2019.
- [88] L. Zhang, B. Wang, X. Li, et al., "Further understanding of the mechanisms of electrochromic devices with variable infrared emissivity based on polyaniline conducting polymers," *J. Mater. Chem. C*, vol. 7, pp. 9878–9891, 2019.
- [89] J. Jensen, M. Hosel, I. Kim, J. S. Yu, J. Jo, and F. C. Krebs, "Fast switching ITO free electrochromic devices," *Adv. Funct. Mater.*, vol. 24, pp. 1228–1233, 2014.
- [90] R. Singh, J. Tharion, S. Murugan, and A. Kumar, "ITO-free solution-processed flexible electrochromic devices based on PEDOT:PSS as transparent conducting electrode," *ACS Appl. Mater. Interfaces*, vol. 9, pp. 19427–19435, 2017.
- [91] W. B. Kang, C. Y. Yan, C. Y. Foo, and P. S. Lee, "Foldable electrochromics enabled by nanopaper transfer method," *Adv. Funct. Mater.*, vol. 25, pp. 4203–4210, 2015.
- [92] H. Z. Li, L. McRae, and A. Y. Elezzabi, "Solution-processed interfacial PEDOT:PSS assembly into porous tungsten molybdenum oxide nanocomposite films for electrochromic applications," *ACS Appl. Mater. Interfaces*, vol. 10, pp. 10520–10527, 2018.
- [93] H. Ling, L. Liu, P. S. Lee, D. Mandler, and X. H. Lu, "Layer-by-layer assembly of PEDOT:PSS and WO<sub>3</sub> nanoparticles: enhanced electrochromic coloration efficiency and mechanism studies by scanning electrochemical microscopy," *Electrochim. Acta*, vol. 174, pp. 57–65, 2015.
- [94] H. Ling, J. L. Lu, S. Phua, et al., "One-pot sequential electrochemical deposition of multilayer poly(3,4-ethylenedioxythiophene):poly(4-styrenesulfonic acid)/tungsten trioxide hybrid films and their enhanced electrochromic properties," *J. Mater. Chem.*, vol. 2, pp. 2708–2717, 2014.
- [95] D. Y. Ma, G. Y. Shi, H. Z. Wang, Q. H. Zhang, and Y. G. Li, "Controllable growth of high-quality metal oxide/conducting polymer hierarchical nanoarrays with outstanding electrochromic properties and solar-heat shielding ability," *J. Mater. Chem.*, vol. 2, pp. 13541–13549, 2014.
- [96] C. J. Barile, D. J. Slotcavage, and M. D. McGehee, "Polymer–nanoparticle electrochromic materials that selectively modulate visible and near-infrared light," *Chem. Mater.*, vol. 28, pp. 1439–1445, 2016.
- [97] S. X. Xiong, S. Y. Yin, Y. Y. Wang, et al., "Organic/inorganic electrochromic nanocomposites with various interfacial interactions: a review," *Mater. Sci. Eng. B*, vol. 221, pp. 41–53, 2017.



- [98] Z. L. Yang, H. T. Pu, and J. L. Yin, "Preparation and electrochromic property of covalently bonded  $\text{WO}_3$ /polyvinylimidazole core-shell microspheres," *J. Colloid Interface Sci.*, vol. 292, pp. 108–112, 2005.
- [99] D. M. DeLongchamp and P. T. Hammond, "Multiple-color electrochromism from layer-by-layer-assembled polyaniline/Prussian Blue nanocomposite thin films," *Chem. Mater.*, vol. 16, pp. 4799–4805, 2004.
- [100] W. S. Liu, X. Y. Zhang, J. Q. Liu, et al., "Electrochromic properties of organic-inorganic composite materials," *J. Alloys Compd.*, vol. 718, pp. 379–385, 2017.
- [101] M. Lahav and M. E. van der Boom, "Polypyridyl metallo-organic assemblies for electrochromic applications," *Adv. Mater.*, vol. 30, p. 1706641, 2018.
- [102] A. Maier, A. R. Rabindranath, and B. Tiede, "Coordinative supramolecular assembly of electrochromic films based on metal ion complexes of polyiminofluorene with terpyridine substituent groups," *Chem. Mater.*, vol. 21, pp. 3668–3676, 2009.
- [103] L. Motiei, M. Lahav, D. Freeman, and M. E. van der Boom, "Electrochromic behavior of a self-propagating molecular-based assembly," *J. Am. Chem. Soc.*, vol. 131, pp. 3468–3469, 2009.
- [104] S. Pai, M. Moos, M. H. Schreck, C. Lambert, and D. G. Kurth, "Green-to-red electrochromic Fe(II) metallo-supramolecular polyelectrolytes self-assembled from fluorescent 2,6-bis(2-pyridyl)pyrroline bithiophene," *Inorg. Chem.*, vol. 56, pp. 1418–1432, 2017.
- [105] M. K. Bera, C. Chakraborty, U. Rana, and M. Higuchi, "Electrochromic Os(II)-based metallo-supramolecular polymers," *Macromol. Rapid Commun.*, vol. 39, p. 1800415, 2018.
- [106] T. R. Gordon, T. Paik, D. R. Klein, et al., "Shape-dependent plasmonic response and directed self-assembly in a new semiconductor building block, indium-doped cadmium oxide (ICO)," *Nano Lett.*, vol. 13, pp. 2857–2863, 2013.
- [107] M. Kanehara, H. Koike, T. Yoshinaga, and T. Teranishi, "Indium tin oxide nanoparticles with compositionally tunable surface plasmon resonance frequencies in the near-IR region," *J. Am. Chem. Soc.*, vol. 131, pp. 17736–17737, 2009.
- [108] Y. Liu, M. Liu, and M. T. Swihart, "Plasmonic copper sulfide-based materials: a brief introduction to their synthesis, doping, alloying, and applications," *J. Phys. Chem. C*, vol. 121, pp. 13435–13447, 2017.
- [109] A. Agrawal, S. H. Cho, O. Zandi, S. Ghosh, R. W. Johns, and D. J. Milliron, "Localized surface plasmon resonance in semiconductor nanocrystals," *Chem. Rev.*, vol. 118, pp. 3121–3207, 2018.
- [110] S. Araki, K. Nakamura, K. Kobayashi, A. Tsuboi, and N. Kobayashi, "Electrochemical optical-modulation device with reversible transformation between transparent, mirror, and black," *Adv. Mater.*, vol. 24, pp. OP122–OP126, 2012.
- [111] A. Tsuboi, K. Nakamura, and N. Kobayashi, "Multicolor electrochromism showing three primary color states (cyan magenta yellow) based on size- and shape-controlled silver nanoparticles," *Chem. Mater.*, vol. 26, pp. 6477–6485, 2014.
- [112] N. Li, P. P. Wei, L. A. Yu, et al., "Dynamically switchable multicolor electrochromic films," *Small*, vol. 15, p. 1804974, 2019.
- [113] B. Tandon, S. Ghosh, and D. J. Milliron, "Dopant selection strategy for high-quality factor localized surface plasmon resonance from doped metal oxide nanocrystals," *Chem. Mater.*, vol. 31, pp. 7752–7760, 2019.
- [114] G. Garcia, R. Buonsanti, E. L. Runnerstrom, et al., "Dynamically modulating the surface plasmon resonance of doped semiconductor nanocrystals," *Nano Lett.*, vol. 11, pp. 4415–4420, 2011.
- [115] Z. C. Wang and G. Chumanov, " $\text{WO}_3$  sol-gel modified Ag nanoparticle arrays for electrochemical modulation of surface plasmon resonance," *Adv. Mater.*, vol. 15, pp. 1285–1289, 2003.
- [116] J. L. Peng, H. H. Jeong, Q. Q. Lin, et al., "Scalable electrochromic nanopixels using plasmonics," *Sci. Adv.*, vol. 5, p. eaaw2205, 2019.
- [117] M. Gugole, O. Olsson, K. L. Xiong, et al., "High-contrast switching of plasmonic structural colors: inorganic versus organic electrochromism," *ACS Photonics*, vol. 7, pp. 1762–1772, 2020.
- [118] E. Hopmann and A. Y. Elezabi, "Plasmochromic nanocavity dynamic light color switching," *Nano Lett.*, vol. 20, pp. 1876–1882, 2020.
- [119] J. Y. Lim, H. C. Ko, and H. Lee, "Systematic prediction of maximum electrochromic contrast of an electrochromic material," *Synth. Met.*, vol. 155, pp. 595–598, 2005.
- [120] J. Padilla, A. M. Osterholm, A. L. Dyer, and J. R. Reynolds, "Process controlled performance for soluble electrochromic polymers," *Sol. Energy Mater. Sol. Cells*, vol. 140, pp. 54–60, 2015.
- [121] J. Padilla, V. Seshadri, G. A. Sotzing, and T. F. Otero, "Maximum contrast from an electrochromic material," *Electrochem. Commun.*, vol. 9, pp. 1931–1935, 2007.
- [122] X. Q. Ju, F. Yang, X. Zhu, and X. L. Jia, "Zinc ion intercalation/deintercalation of metal organic framework-derived nanostructured  $\text{NiO@C}$  for low-transmittance and high-performance electrochromism," *ACS Sustain. Chem. Eng.*, vol. 8, pp. 12222–12229, 2020.
- [123] M. H. Wang, Y. Chen, B. W. Gao, and H. Lei, "Electrochromic properties of nanostructured  $\text{WO}_3$  thin films deposited by glancing-angle magnetron sputtering," *Adv. Electron Mater.*, vol. 5, p. 1800713, 2019.
- [124] R. Ayranci, G. Baskaya, M. Guzel, et al., "Enhanced optical and electrical properties of PEDOT via nanostructured carbon materials: a comparative investigation," *Nano Struct. Nano Objects*, vol. 11, pp. 13–19, 2017.
- [125] M. R. J. Scherer, L. Li, P. M. S. Cunha, O. A. Scherman, and U. Steiner, "Enhanced electrochromism in gyroid-structured vanadium pentoxide," *Adv. Mater.*, vol. 24, pp. 1217–1221, 2012.
- [126] H. Z. Li, J. W. Chen, M. Q. Cui, et al., "Spray coated ultrathin films from aqueous tungsten molybdenum oxide nanoparticle ink for high contrast electrochromic applications," *J. Mater. Chem. C*, vol. 4, pp. 33–38, 2016.
- [127] D. S. Dalavi, M. J. Suryavanshi, D. S. Patil, et al., "Nanoporous nickel oxide thin films and its improved electrochromic performance: effect of thickness," *Appl. Surf. Sci.*, vol. 257, pp. 2647–2656, 2011.
- [128] G. Tahtali, Z. Has, C. Doyranli, C. Varlikli, and S. Koyuncu, "Solution processable neutral state colourless electrochromic devices: effect of the layer thickness on the electrochromic performance," *J. Mater. Chem. C*, vol. 4, pp. 10090–10094, 2016.
- [129] B. W. C. Au, K. Y. Chan, and D. Knipp, "Effect of film thickness on electrochromic performance of sol-gel deposited tungsten oxide ( $\text{WO}_3$ )," *Opt. Mater.*, vol. 94, pp. 387–392, 2019.

- [130] F. Hu, B. Yan, E. H. Ren, et al., “Constructing spraying-processed complementary smart windows via electrochromic materials with hierarchical nanostructures,” *J. Mater. Chem. C*, vol. 7, pp. 14855–14860, 2019.
- [131] W. Zhang, X. Chen, X. Wang, S. Zhu, S. Wang, and Q. Wang, “Pulsed electrodeposition of nanostructured polythiophene film for high-performance electrochromic devices,” *Sol. Energy Mater. Sol. Cells*, vol. 219, p. 110775, 2021.
- [132] D. R. Sahu, T. J. Wu, S. C. Wang, and J. L. Huang, “Electrochromic behavior of NiO film prepared by e-beam evaporation,” *J. Sci. Adv. Mater. Devices*, vol. 2, pp. 225–232, 2017.
- [133] I. Sorar, E. Pehlivan, G. A. Niklasson, and C. G. Granqvist, “Electrochromism of DC magnetron-sputtered TiO<sub>2</sub>: role of film thickness,” *Appl. Surf. Sci.*, vol. 318, pp. 24–27, 2014.
- [134] C. G. Wu, M. I. Lu, S. J. Chang, and C. S. Wei, “A solution-processable high-coloration-efficiency low-switching-voltage electrochromic polymer based on polycyclopentadithiophene,” *Adv. Funct. Mater.*, vol. 17, pp. 1063–1070, 2007.
- [135] D. Ma, G. Shi, H. Wang, Q. Zhang, and Y. Li, “Morphology-tailored synthesis of vertically aligned 1D WO<sub>3</sub> nano-structure films for highly enhanced electrochromic performance,” *J. Mater. Chem.*, vol. 1, pp. 684–691, 2013.
- [136] D. Ma, H. Wang, Q. Zhang, and Y. Li, “Self-weaving WO<sub>3</sub> nanoflake films with greatly enhanced electrochromic performance,” *J. Mater. Chem.*, vol. 22, pp. 16633–16639, 2012.
- [137] M. A. Arvizu, H. Y. Qu, U. Cindemir, et al., “Electrochromic WO<sub>3</sub> thin films attain unprecedented durability by potentiostatic pretreatment,” *J. Mater. Chem.*, vol. 7, pp. 2908–2918, 2019.
- [138] R. C. D. Peres, V. F. Juliano, M. A. Depaoli, S. Panero, and B. Scrosati, “Electrochromic properties of dodecylbenzenesulfonate doped poly(pyrrole),” *Electrochim. Acta*, vol. 38, pp. 869–876, 1993.
- [139] L. P. Hao, W. Wang, H. J. Niu, and Y. Zhou, “Grafting triphenylamine groups onto polysiloxanes to improve interaction between the electrochromic films and ITO,” *Electrochim. Acta*, vol. 246, pp. 259–268, 2017.
- [140] Z. H. Jiao, X. W. Sun, J. M. Wang, L. Ke, and H. V. Demir, “Hydrothermally grown nanostructured WO<sub>3</sub> films and their electrochromic characteristics,” *J. Phys. D Appl. Phys.*, vol. 43, p. 285501, 2010.
- [141] T. T. Ye, Y. Sun, X. Zhao, B. P. Lin, H. Yang, and X. Q. Zhang, “Long-term-stable, solution-processable, electrochromic carbon nanotubes/polymer composite for smart supercapacitor with wide working potential window,” *J. Mater. Chem.*, vol. 6, pp. 18994–19003, 2018.
- [142] J. M. Berak and M. J. Sienko, “Effect of oxygen-deficiency on electrical transport properties of tungsten trioxide crystals,” *J. Solid State Chem.*, vol. 2, pp. 109–133, 1970.
- [143] L. Y. Su, L. G. Zhang, J. H. Fang, M. H. Xu, and Z. H. Lu, “Electrochromic and photoelectrochemical behavior of electrodeposited tungsten trioxide films,” *Sol. Energy Mater. Sol. Cells*, vol. 58, pp. 133–140, 1999.
- [144] P. R. Somani and S. Radhakrishnan, “Electrochromic materials and devices: present and future,” *Mater. Chem. Phys.*, vol. 77, pp. 117–133, 2003.
- [145] S. K. Deb, “A novel electrophotographic system,” *Appl. Opt.*, vol. 8, pp. 192–195, 1969.
- [146] L. Zhang, D. L. Chao, P. H. Yang, et al., “Flexible pseudocapacitive electrochromics via inkjet printing of additive-free tungsten oxide nanocrystal ink,” *Adv. Energy Mater.*, vol. 10, p. 2000142, 2020.
- [147] J. Zhang, J. P. Tu, X. H. Xia, X. L. Wang, and C. D. Gu, “Hydrothermally synthesized WO<sub>3</sub> nanowire arrays with highly improved electrochromic performance,” *J. Mater. Chem.*, vol. 21, pp. 5492–5498, 2011.
- [148] A. Azam, J. Kim, J. Park, et al., “Two-dimensional WO<sub>3</sub> nanosheets chemically converted from layered WS<sub>2</sub> for high-performance electrochromic devices,” *Nano Lett.*, vol. 18, pp. 5646–5651, 2018.
- [149] S. Adhikari and D. Sarkar, “High efficient electrochromic WO<sub>3</sub> nanofibers,” *Electrochim. Acta*, vol. 138, pp. 115–123, 2014.
- [150] Y. Q. Li, W. A. McMaster, H. Wei, D. H. Chen, and R. A. Caruso, “Enhanced electrochromic properties of WO<sub>3</sub> nanotree-like structures synthesized via a two-step solvothermal process showing promise for electrochromic window application,” *ACS Appl. Nano Mater.*, vol. 1, pp. 2552–2558, 2018.
- [151] S. Cong, Y. Y. Tian, Q. W. Li, Z. G. Zhao, and F. X. Geng, “Single-crystalline tungsten oxide quantum dots for fast pseudocapacitor and electrochromic applications,” *Adv. Mater.*, vol. 26, pp. 4260–4267, 2014.
- [152] Y. J. Yao, Q. Zhao, W. Wei, et al., “WO<sub>3</sub> quantum-dots electrochromism,” *Nano Energy*, vol. 68, p. 104350, 2020.
- [153] H. Z. Li, G. Y. Shi, H. Z. Wang, Q. H. Zhang, and Y. G. Li, “Self-seeded growth of nest-like hydrated tungsten trioxide film directly on FTO substrate for highly enhanced electrochromic performance,” *J. Mater. Chem.*, vol. 2, pp. 11305–11310, 2014.
- [154] S. R. Bathe and P. S. Patil, “Influence of Nb doping on the electrochromic properties of WO<sub>3</sub> films,” *J. Phys. D Appl. Phys.*, vol. 40, pp. 7423–7431, 2007.
- [155] S. J. Xie, Z. J. Bi, Y. B. Chen, et al., “Electrodeposited Mo-doped WO<sub>3</sub> film with large optical modulation and high areal capacitance toward electrochromic energy-storage applications,” *Appl. Surf. Sci.*, vol. 459, pp. 774–781, 2018.
- [156] B. R. Koo, K. H. Kim, and H. J. Ahn, “Switching electrochromic performance improvement enabled by highly developed mesopores and oxygen vacancy defects of Fe-doped WO<sub>3</sub> films,” *Appl. Surf. Sci.*, vol. 453, pp. 238–244, 2018.
- [157] Y. Zhan, M. R. J. Tan, X. Cheng, et al., “Ti-doped WO<sub>3</sub> synthesized by a facile wet bath method for improved electrochromism,” *J. Mater. Chem. C*, vol. 5, pp. 9995–10000, 2017.
- [158] M. A. Arvizu, G. A. Niklasson, and C. G. Granqvist, “Electrochromic W<sub>1-x-y</sub>Ti<sub>x</sub>Mo<sub>y</sub>O<sub>3</sub> thin films made by sputter deposition: large optical modulation, good cycling durability, and approximate color neutrality,” *Chem. Mater.*, vol. 29, pp. 2246–2253, 2017.
- [159] A. Arash, S. A. Tawfik, M. J. S. Spencer, et al., “Electrically activated UV-A filters based on electrochromic MoO<sub>3-x</sub>,” *ACS Appl. Mater. Interfaces*, vol. 12, pp. 16997–17003, 2020.
- [160] S. Santhosh, M. Mathankumar, S. S. Chandrasekaran, A. K. N. Kumar, P. Murugan, and B. Subramanian, “Effect of ablation rate on the microstructure and electrochromic properties of pulsed-laser-deposited molybdenum oxide thin films,” *Langmuir*, vol. 33, pp. 19–33, 2017.
- [161] L. Zheng, Y. Xu, D. Jin, and Y. Xie, “Novel metastable hexagonal MoO<sub>3</sub> nanobelts: synthesis, photochromic, and electrochromic properties,” *Chem. Mater.*, vol. 21, pp. 5681–5690, 2009.
- [162] T. G. Novak, J. Kim, A. P. Tiwari, et al., “2D MoO<sub>3</sub> nanosheets synthesized by exfoliation and oxidation of MoS<sub>2</sub> for high

- contrast and fast response time electrochromic devices,” *ACS Sustain. Chem. Eng.*, vol. 8, pp. 11276–11282, 2020.
- [163] N. N. Dinh, N. T. T. Oanh, P. D. Long, M. C. Bernard, and A. H. L. Goff, “Electrochromic properties of  $\text{TiO}_2$  anatase thin films prepared by a dipping sol-gel method,” *Thin Solid Films*, vol. 423, pp. 70–76, 2003.
- [164] E. Silik, S. Pat, S. Ozen, et al., “Electrochromic properties of  $\text{TiO}_2$  thin films grown by thermionic vacuum arc method,” *Thin Solid Films*, vol. 640, pp. 27–32, 2017.
- [165] Z. Tong, S. Liu, X. Li, L. Mai, J. Zhao, and Y. Li, “Achieving rapid Li-ion insertion kinetics in  $\text{TiO}_2$  mesoporous nanotube arrays for bifunctional high-rate energy storage smart windows,” *Nanoscale*, vol. 10, pp. 3254–3261, 2018.
- [166] J. Z. Chen, W. Y. Ko, Y. C. Yen, P. H. Chen, and K. J. Lin, “Hydrothermally processed  $\text{TiO}_2$  nanowire electrodes with antireflective and electrochromic properties,” *ACS Nano*, vol. 6, pp. 6633–6639, 2012.
- [167] L. De Trizio, R. Buonsanti, A. M. Schimpf, et al., “Nb-doped colloidal  $\text{TiO}_2$  nanocrystals with tunable infrared absorption,” *Chem. Mater.*, vol. 25, pp. 3383–3390, 2013.
- [168] S. Cao, S. L. Zhang, T. R. Zhang, and J. Y. Lee, “Fluoride-assisted synthesis of plasmonic colloidal Ta-doped  $\text{TiO}_2$  nanocrystals for near-infrared and visible-light selective electrochromic modulation,” *Chem. Mater.*, vol. 30, pp. 4838–4846, 2018.
- [169] S. Cao, S. L. Zhang, T. R. Zhang, Q. F. Yao, and J. Y. Lee, “A visible light-near-infrared dual-band smart window with internal energy storage,” *Joule*, vol. 3, pp. 1152–1162, 2019.
- [170] C. Costa, C. Pinheiro, I. Henriques, and C. A. T. Laia, “Electrochromic properties of inkjet printed vanadium oxide gel on flexible polyethylene terephthalate/indium tin oxide electrodes,” *ACS Appl. Mater. Interfaces*, vol. 4, pp. 5266–5275, 2012.
- [171] D. Wei, M. R. J. Scherer, C. Bower, P. Andrew, T. Ryhanen, and U. Steiner, “A nanostructured electrochromic supercapacitor,” *Nano Lett.*, vol. 12, pp. 1857–1862, 2012.
- [172] Y. Y. Cui, Y. J. Ke, C. Liu, et al., “Thermochromic  $\text{VO}_2$  for energy-efficient smart windows,” *Joule*, vol. 2, pp. 1707–1746, 2018.
- [173] I. Mjejri, M. Gaudon, G. Song, C. Labrugere, and A. Rougier, “Crystallized  $\text{V}_2\text{O}_5$  as oxidized phase for unexpected multicolor electrochromism in  $\text{V}_2\text{O}_3$  thick film,” *ACS Appl. Energy Mater.*, vol. 1, pp. 2721–2729, 2018.
- [174] I. Mjejri and A. Rougier, “Color switching in  $\text{V}_3\text{O}_7\text{-H}_2\text{O}$  films cycled in Li and Na based electrolytes: novel vanadium oxide based electrochromic materials,” *J. Mater. Chem. C*, vol. 8, pp. 3631–3638, 2020.
- [175] M. M. Margoni, S. Mathuri, K. Ramamurthi, R. R. Babu, V. Ganesh, and K. Sethuraman, “Hydrothermally grown nano and microstructured  $\text{V}_2\text{O}_5$  thin films for electrochromic application,” *Appl. Surf. Sci.*, vol. 449, pp. 193–202, 2018.
- [176] F. Lin, D. Nordlund, T. C. Weng, et al., “Hole doping in Al-containing nickel oxide materials to improve electrochromic performance,” *ACS Appl. Mater. Interfaces*, vol. 5, pp. 301–309, 2013.
- [177] Q. R. Liu, G. B. Dong, Y. Xiao, M. P. Delplancke-Ogletree, F. Reniers, and X. G. Diao, “Electrolytes-relevant cyclic durability of nickel oxide thin films as an ion-storage layer in an all-solid-state complementary electrochromic device,” *Sol. Energy Mater. Sol. Cells*, vol. 157, pp. 844–852, 2016.
- [178] K. K. Purushothaman and G. Muralidharan, “Nanostructured  $\text{NiO}$  based all solid state electrochromic device,” *J. Sol. Gel Sci. Technol.*, vol. 46, pp. 190–194, 2008.
- [179] R. A. Patil, R. S. Devan, J. H. Lin, Y. R. Ma, P. S. Patil, and Y. Liou, “Efficient electrochromic properties of high-density and large-area arrays of one-dimensional  $\text{NiO}$  nanorods,” *Sol. Energy Mater. Sol. Cells*, vol. 112, pp. 91–96, 2013.
- [180] J. H. Zhang, G. F. Cai, D. Zhou, et al., “Co-doped  $\text{NiO}$  nanoflake array films with enhanced electrochromic properties,” *J. Mater. Chem. C*, vol. 2, pp. 7013–7021, 2014.
- [181] G. F. Cai, P. Darmawan, M. Q. Cui, et al., “Inkjet-printed all solid-state electrochromic devices based on  $\text{NiO}/\text{WO}_3$  nanoparticle complementary electrodes,” *Nanoscale*, vol. 8, pp. 348–357, 2016.
- [182] S. Moghe, A. D. Acharya, R. Panda, et al., “Effect of copper doping on the change in the optical absorption behaviour in  $\text{NiO}$  thin films,” *Renew. Energy*, vol. 46, pp. 43–48, 2012.
- [183] C. R. Dhas, R. Venkatesh, R. Sivakumar, A. M. E. Raj, and C. Sanjeeviraja, “Fast electrochromic response of porous-structured cobalt oxide ( $\text{Co}_3\text{O}_4$ ) thin films by novel nebulizer spray pyrolysis technique,” *Ionics*, vol. 22, pp. 1911–1926, 2016.
- [184] H. S. Shim, V. R. Shinde, H. J. Kim, Y. E. Sung, and W. B. Kim, “Porous cobalt oxide thin films from low temperature solution phase synthesis for electrochromic electrode,” *Thin Solid Films*, vol. 516, pp. 8573–8578, 2008.
- [185] X. H. Xia, J. P. Tu, J. Zhang, X. H. Huang, X. L. Wang, and X. B. Zhao, “Improved electrochromic performance of hierarchically porous  $\text{Co}_3\text{O}_4$  array film through self-assembled colloidal crystal template,” *Electrochim. Acta*, vol. 55, pp. 989–994, 2010.
- [186] X. H. Xia, J. P. Tu, J. Zhang, J. Y. Xiang, X. L. Wang, and X. B. Zhao, “Cobalt oxide ordered bowl-like array films prepared by electrodeposition through monolayer polystyrene sphere template and electrochromic properties,” *ACS Appl. Mater. Interfaces*, vol. 2, pp. 186–192, 2010.
- [187] K. R. Li, Q. H. Zhang, H. Z. Wang, and Y. G. Li, “Red, Green, Blue (RGB) Electrochromic fibers for the new smart color change fabrics,” *ACS Appl. Mater. Interfaces*, vol. 6, pp. 13043–13050, 2014.
- [188] H. W. Fan, K. R. Li, X. L. Liu, et al., “Continuously processed, long electrochromic fibers with multi-environmental stability,” *ACS Appl. Mater. Interfaces*, vol. 12, pp. 28451–28460, 2020.